

STIMULATED BRILLOUIN SCATTERING SWITCHING IN MID  
INFRARED FIBERS

Final Report

By  
Chung Yu

Sept 15, 1992

U.S. ARMY RESEARCH OFFICE  
DAAL03-88-G-0005

FORM 302 (REV. 12-13-82) UNCLASSIFIED 3

NORTH CAROLINA A&T STATE UNIVERSITY  
GREENSBORO, NC 27411

Accession For	
NTIS CRA&I	<input checked="" type="checkbox"/>
DTIC TAB	<input type="checkbox"/>
Unannounced	<input type="checkbox"/>
Justification	
By	
Date	
Availability Codes	
Avail and/or	
Special	
A-1	

AD-A260 456

MENTATION PAGE

Form Approved  
OMB No. 0704-0188

2



estimated to average 1 hour per response, including the time for reviewing instructions, searching existing data sources, and reviewing the collection of information. Send comments regarding this burden estimate or any other aspect of this burden to Washington Headquarters Services, Directorate for Information Operations and Reports, 1215 Jefferson Davis Drive, Office of Management and Budget, Paperwork Reduction Project (0704-0188), Washington, DC 20503

REPORT DATE

3. REPORT TYPE AND DATES COVERED

Oct 92

Final 1 Jan 88-15 Aug 92

4. TITLE AND SUBTITLE

Stimulated Brillouin Scattering Switching in Mid Fibers

5. FUNDING NUMBERS

DA4L03-88-G-0005

6. AUTHOR(S)

Chung Yu

DTIC  
ELECTE

7. PERFORMING ORGANIZATION NAME(S) AND ADDRESS(ES)

North Carolina A&T State Univ  
Greensboro, NC 27411

FEB 19 1993

8. PERFORMING ORGANIZATION REPORT NUMBER

9. SPONSORING / MONITORING AGENCY NAME(S) AND ADDRESS(ES)

U. S. Army Research Office  
P. O. Box 12211  
Research Triangle Park, NC 27709-2211

10. SPONSORING / MONITORING AGENCY REPORT NUMBER

ARO 25197.1-EL-H

11. SUPPLEMENTARY NOTES

The view, opinions and/or findings contained in this report are those of the author(s) and should not be construed as an official Department of the Army position, policy, or decision, unless so designated by other documentation.

12a. DISTRIBUTION / AVAILABILITY STATEMENT

Approved for public release; distribution unlimited.

12b. DISTRIBUTION CODE

13. ABSTRACT (Maximum 200 words)

This report contains a brief outline of research findings plus a description of the experimental design, a discussion of switching of optical signal by Stimulated Brillouin scattering single-mode optical fibers and a preliminary study of fiber ring for enhancement of SBS generation in mid IR Fiber.

93-03402



14. SUBJECT TERMS

Infrared Fibers, Brillouin Scattering, Optical Fibers, Optical Signals, Switch Systems

15. NUMBER OF PAGES

65

16. PRICE CODE

17. SECURITY CLASSIFICATION OF REPORT

UNCLASSIFIED

18. SECURITY CLASSIFICATION OF THIS PAGE

UNCLASSIFIED

19. SECURITY CLASSIFICATION OF ABSTRACT

UNCLASSIFIED

20. LIMITATION OF ABSTRACT

UL

## TABLE OF CONTENTS

### Brief Outline of Research Findings

1.	Introduction	1
1.1.	Comparison of SBS phenomena	1
1.2.	SBS Threshold	3
1.3.	Conditions for Excitation of SBS	4
1.4.	Mid Infrared Fibers	7
1.5.	SBS in Infrared Fibers at 10.6 $\mu\text{m}$	13
1.6.	Typical Characteristic of SBS	14
1.7.	Proposed Experimental Setup to Observe Mode Patterns	16
2.	Experimental Design and Results	18
2.1.	Introduction	18
2.2.	Experimental Setup	23
2.3.	Field Patterns in Waveguide	25
2.4.	Experimental Results	28
2.4.1.	Frequency Response of Waveguide	28
2.4.2.	Phonon Detection	29
2.4.3.	Injection of External Radiation	30
2.4.4.	Transmitted Pulse	33
2.5.	Consideration for Improvements in Experimental Design	35
3.	Switching of Optical Signal by Stimulated Brillouin Scattering Single-mode Optical Fibers	37
3.1.	Conventional Switches	37
3.2.	Theory of SBS Based All-optical Switches	37
3.3.	Design and Testing of a Prototype SBS-based Switch	40

3.4.	Design of Implementation SBS Based Switch	41
3.4.1.	The Commercially Available SBS Based Optical Switch System	42
3.4.2.	The All Fiber-based SBS Optical Switch System	43
4.	Preliminary Study of Fiber Ring for Enhancement of SBS Generation in Mid IR Fiber	45
4.1.	Introduction	45
4.2.	SBS Ring in the Near and Mid IR	46
4.3.	Evaluation of Performance Parameters of SBS Fiber Ring	48
4.4.	Simulation Results	51
	<b>Bibliography</b>	<b>59</b>
	<b>Publications Resulting from the Grant</b>	<b>63</b>
	<b>Scientific Personnel Supported Directly or Indirectly by the Grant</b>	<b>65</b>

## BRIEF OUTLINE OF RESEARCH FINDINGS

Transition to the near IR has been prompted by the immaturity of fiber technology in the mid IR. Attempts at implementing some of the concepts proposed have been further enhanced by the installation of a fiber ring, which is predicted to greatly lower the SBS threshold. In the course of study of the SBS fiber amplifier, the question of noise emerges as a key issue. When the SBS process in the fiber is viewed as an amplifying mechanism, then Brillouin noise, which is thermal and mechanical in nature, is presumably detrimental to the amplifying process. Our efforts have thus been to reduce such noise by the application of the fiber ring, which has low noise properties. However, when such thermally and mechanically generated noise in a linear fiber due to the ambient is selectively amplified, then such a fiber system when closely coupled to the ambient, or a structure of some kind, may serve as an excellent ambient noise sensing element. When this sensing element is coupled to a low noise coherent Brillouin amplifying fiber ring, then the sensing system may prove to be robust and fault tolerant. The key element in this case is the Brillouin amplifying process as derived from a fiber ring. It is thus remarkable that the same Brillouin process may be used both for optical amplification and optical sensing with features not yet suggested by any researcher in this field.

In our endeavor to return to the mid IR, there seems to be some degree of improving prospect with recent announcement of the availability of commercial chalcogenide fibers with less than 1 db/m loss in the 6-9  $\mu\text{m}$  region, and less than 4 db/m at 10.6  $\mu\text{m}$ . Such fibers are adequate for application in Attenuated Total Reflectance (ATR) studies of the structure of liquids. This group is contemplating some efforts in this direction by the installation of these fibers in place of conventional Cassegrainian optics and ATR cells. Further mid IR technology advancement is still anticipated in order that such a fiber ring can be constructed to further lower SBS threshold, the key to the fabrication of mid IR optical active devices.

## CHAPTER 1 INTRODUCTION

Our study of SBS incorporates the detection of phonons by imposing external radiation on the nonlinear medium placed in a suitable waveguide structure. The reported detection of phonon emissions and modulation of the transmitted and reflected laser pulse by the injected radiation[1] had encouraged us to undertake a systematic study of this effect. An experimental scheme was devised to study this effect. This study has engineering implications and profound consequences in the investigation of optical switching in fibers using external sources or control mechanisms in the mid infrared range.

A theoretical analysis of Stimulated Brillouin Scattering together with a comparison of SBS parameters achieved by several groups were given. This comparison provided us with a better understanding of the effect of SBS achieved at longer wavelengths. The typical characteristics of SBS were discussed. Potential applications of optical switches using nonlinear phenomena were also discussed, in addition to the comparison of switching at near and mid infrared wavelength.

The power density distribution of light in the core of the fiber for various modes describes the mode patterns that are characteristic of the modes. This knowledge can be applied to verifying SBS phenomena by observing the changes in the mode patterns of the transmitted pulse. Pump depletion is a well known manifestation of SBS process. At the onset of SBS, the transmitted pump energy would have coupled to the stokes wave, and the resulting depletion has a spatial profile characteristic. This characteristic can be monitored by using thermal image plates, and the changes in spatial profile due to SBS can be compared with the established mode patterns of the fiber.

### 1.1 Comparison of SBS phenomena

SBS phenomena in optical fibers have been cited by several research groups. These phenomena were observed at different wavelengths and threshold power[2], as summarized in Table 1.1. Distinct parameters to be noted are microwave shift due to SBS, the fiber length, and the linear loss of the fiber.

The fiber length and its linear loss are an important factors in determining the

threshold power of SBS. The effective interaction length is given by

$$L_e = \frac{1}{\alpha} [1 - e^{-\alpha L}] \quad (1.1)$$

where  $\alpha$  is the absorption coefficient  $m^{-1}$ , and  $L$  is the fiber length. For long fibers, i.e.  $\alpha L \gg 1$ , the effective interaction is reduced to  $1/\alpha$ ; if  $\alpha$  is very small and finite length,  $L$ , then  $L_e \approx L$ .

Research Group	Wave-length ( $\mu m$ )	Frequenc y shift (GHz)	Fiber Length/ Made	Linear Loss (dB/Km)	Diameter ( $\mu m$ )	SBS Threshold
Ippen & Stolen	0.5335	32.2	5.8 m glass	1300	3.8	2.3 W
Edge et al	1.064	16.1	0.2 silica	-	9	200 W
Cotter	1.32	13.1	13.6 Km silica	0.41	9	5.6 mW
Kovalev et al	10.6	0.9	0.65 m KRS-5	868	1000	17 kW
C. Yu C. Fong	10.6	2 MHz 1 GHz	1 m AgCl	1336	700	17 kW

Table 1.1: Observation of SBS phenomena by several research groups

The efficiency of the nonlinear interaction in bulk medium is the product of the interaction length and focal intensity, and is given by

$$E = \frac{P}{\pi \omega^2} \times \frac{\pi \omega^2}{\lambda} = \frac{P}{\lambda} \quad (1.2)$$

where  $P$  is the input power,  $\omega^2$  is the beam spot of radius  $\omega$ , and  $\lambda$  is the wavelength of light. Since Eq. (1.2) is independent of length, greater efficiency cannot be achieved by using longer samples of bulk material. However, with the waveguiding properties of an optical fiber, the intensity in a small focal spot can be maintained over longer distances. Hence, the efficiency of the nonlinear interaction can be increased by using an optical fiber, and the

larger the efficiency the stronger would be the SBS coupling and the lower the threshold for the onset of SBS.

With an effective interaction length, the efficiency is now given by

$$E = \frac{P}{\pi \omega^2} \times L_e \quad (1.3)$$

For sufficiently long fibers, E would be inversely proportional to the linear loss of the fibers. By assuming the beam waist to be approximately the fiber radius, the efficiency of Cotter's fiber is about  $6.69 \times 10^{11}$ , while the Yu's fiber is about  $3.79 \times 10^{10}$ . The efficiency of Cotter's fiber is about 18 times larger, mainly because of his low-loss fiber which permits a longer effective interaction length. However, by judging the experimental efficiency which is defined as the product of the actual laser power and fiber length used to achieve threshold, the Yu's fiber is 17000 W-m while Cotter's fiber is 76 W-m. This indicates the fact that the SBS coupling is much stronger in mid IR fiber than in silicate fiber. In other words, the mid-IR region is highly phonon active.

## 1.2 SBS Threshold

The exponential gain[3] along a fiber of length L is given by

$$G = g_B I L_e \quad (1.4)$$

where  $g_B$  is the gain coefficient (cm/MW) characteristic of the material, I is the intensity of the exciting radiation (MW/cm<sup>2</sup>). The threshold power for SBS can be estimated from

$$P = AI = \frac{GA}{g_B L_e} \quad (1.5)$$

where A is the effective interaction area of the guide mode.

According to Smith[3], the exponential gain needed for the spontaneous intensity to reach the pump level for a long low-loss optical fiber is  $G=21$ . Thus, the threshold power is approximately given as

$$P = 21 \frac{A}{g_B L_e} \quad (1.6)$$

The numerical factor  $G=21$  was approximated for a wavelength in the visible or near IR region. However, in the mid infrared region of  $10.6 \mu\text{m}$  and by the fact that the intensity of the spontaneous excited radiation is proportional to  $\lambda^{-4}$ , the numerical value of  $G$  needed to achieve threshold is about 36.

From actual experiments performed by Kovalev[4] to observe SBS in KRS-5 fiber at  $10.6 \mu\text{m}$ , he approximated the exponential gain to be 28 in order for steady state SBS to occur. Therefore,  $G$  is taken to be 28 for the approximation of SBS threshold power in the mid IR region.

### 1.3 Conditions for Excitation of SBS

The factors for excitation of SBS include the duration and linewidth of light sources which strongly influence the scattering process, the SBS gain coefficient which is a characteristic of the material medium, and also the linear loss, effective interaction area, and the intensity of the light source.

The SBS gain coefficient is given by

$$g_B = \frac{\Upsilon_e^2 \omega_s^2}{c^3 \eta \rho_o V_s \Gamma_B}$$

The electrostrictive coefficient  $\Upsilon_e$  is given by the tensor

$$\Upsilon_e = |\epsilon p \epsilon|$$

which can be calculated from the Lorentz law and having the form[5]

$$\epsilon p \epsilon = \frac{1}{3} (\epsilon - 1) (\epsilon + 2) \quad (1.7)$$

where  $\epsilon = n^2$  is the permittivity tensor, and  $p$  is the tensor of photoelastic constant of the medium. Hence, the electrostrictive coefficient is approximately given by  $\Upsilon_e^2 = p^2 \eta^8$ . The gain

coefficient can be rewritten as

$$g_B = \frac{2\pi n^7 p^2}{c\lambda^2 \rho_o V_a \Delta v_B} \quad (1.8)$$

where we have replaced  $\Gamma_B = 2\Pi\Delta v_B$  and  $\omega_s^2 = 4\Pi^2 c^2 / \lambda^2$ .

The lifetime of acoustic phonons  $\tau_B = 1/\Gamma_B$  depends (in many cases) quadratically on the inverse of its wavevector  $k_B$ [6]:

$$\tau_B = \frac{\rho_o}{\eta_s k_B^2} = \frac{\rho_o}{4\eta_s k_L^2 (\theta/2)} \quad (1.9)$$

where  $\eta_s$  is the viscosity. Since  $k_L$  is inversely proportional to  $\lambda$ , therefore  $\tau_B \propto \lambda^2$  and leads to  $\Delta v_B \propto \lambda^{-2}$ . Hence, we can say that  $g_B$  is independent of wavelength and proportional to the seventh power of the refractive index of the medium. For a small scattering angle, light is scattered in the forward direction by phonons of lower frequency and consequently longer phonon lifetime, according to Eq. (1.9).

In terms of relative gain between forward and backward SBS, a small scattering angle results in a larger forward gain. Hence, the angle-dependent gain and phonon lifetime would favor forward SBS interaction when a long pump pulse is used. For short pulses, forward SBS will not build up. It was pointed out analytically that intensity of the forward scattered light would reach the intensity of the backward scattered light at several phonons lifetime later. The schematic view of the forward and backward SBS interaction in terms of intensity and phonon lifetime is shown in Fig. 1.1. Based on energy conservation principles, backward SBS may cutoff because of the high forward SBS gain. This means that the stokes wave is copropagating with the pump, but carries most of the energy.

The phonon lifetime determines the maximum duration of the laser pulse,  $t_o$ , and consequently, the linewidth  $\Delta v$ . In order to achieve a steady-state SBS, the duration and linewidth of the laser pulse must satisfy the conditions[5]:

$$t_o \geq G\tau_B \quad (1.10)$$

$$\Delta V_s \frac{\Delta v_B}{Gc} = \frac{1}{G\tau_B c} \quad (1.11)$$

where  $\Delta v_B$  is the linewidth of the spontaneous Brillouin scattering.

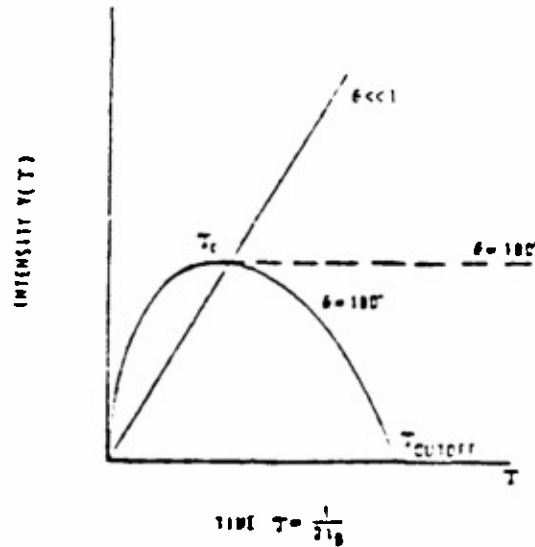


Figure 1.1: Schematic view of backward SBS cutoff due to onset of FSBS[after 7].

Table 1.2 shows the various material mediums and their associated refractive indices, steady-state SBS gains, acoustic frequencies, and phonon lifetimes. The time duration to establish steady-state SBS for all materials ranging from  $\approx 0.7 \mu s$  for Ge and  $\approx 20 \mu s$  for GaAs. For

Material	n (10.6 $\mu m$ )	$V_B$ ( $10^5$ cm/s)	g (cm/MW)	$\tau$ ( $\mu s$ )
Ge	4	5.48	0.18	0.02
GaAs	3.27	1.90	3.32	0.55
KRS-5	2.37	2.08	0.075	0.17
KRS-6	2.17	2.42	0.055	0.25
ZnSe	2.41	4.50	0.035	0.15

Table 1.2: Optical medium and their SBS characteristics. After Kovalev[5]

a pulse duration which is less than the time constant, the minimum threshold power for

excitation of SBS would increase. Other factor that would increase the threshold by virtue of the pump spectrum is when  $\Delta\nu > \Delta\nu_B$ , i.e. when the laser linewidth is broader than the spontaneous Brillouin linewidth. In this case the gain coefficient would be reduced to

$$g_B = G \frac{\Delta\nu_B}{\Delta\nu_l} \quad (1.12)$$

Also, the depolarization which occurs in most optical fibers will reduce the gain by a factor of 2.

#### 1.4 Mid Infrared Fibers

In recent years there has been a considerable interest in developing optical fibers that are transparent to infrared radiation. This is due to the fact that in some materials the linear losses in the mid infrared range (2-10  $\mu\text{m}$ ) can be very low:  $10^{-2}$  dB/km or even less[8].

IR Material	Fiber Type	Attenuation (dB/km)	Potential Attenuation (dB/km)
AgBr	Single-crystal*	~ 9000 @ 10.6 $\mu\text{m}$	$10^{-3}$ @ 5 $\mu\text{m}$
AgCl	Polycrystalline*	~ 6000 @ 14 $\mu\text{m}$	$10^{-3}$ @ 5 $\mu\text{m}$
KRS-5	Polycrystalline*	~ 300 @ 10.6 $\mu\text{m}$	$10^{-3}$ @ 7 $\mu\text{m}$
TlBr	Polycrystalline*	~ 400 @ 10.6 $\mu\text{m}$	$10^{-4}$ @ 7 $\mu\text{m}$
KCl	Polycrystalline*	~ 4000 @ 10.6 $\mu\text{m}$	$10^{-4}$ @ 5 $\mu\text{m}$
Chalcogenide	Glass	~ 10,000 @ 6.5 $\mu\text{m}$	$10^{-2}$ @ 4.5 $\mu\text{m}$
Fluorohafnate	Glass	~ 300 @ 3.6 $\mu\text{m}$	$10^{-3}$ @ 3.5 $\mu\text{m}$
Fluorozirconate	Glass	~ 300 @ 3.6 $\mu\text{m}$	$10^{-3}$ @ 3.5 $\mu\text{m}$
Heavy Metal Fluoride	Glass	~ 2000 @ 3.5 $\mu\text{m}$	$10^{-3}$ @ 3.5 $\mu\text{m}$

\* indicates uncladded fiber

Table 1.3: Reported attenuations and theoretical predictions of attenuation in infrared fibers (from Laser & Optonics).

The comparison of attenuations reported for infrared fibers with theoretical predictions of attenuation is shown in table 1.3. Fig.1.2 shows the theoretical minimum loss curves for several infrared fiber materials. Another factor for using longer wavelength is that of the strong decrease in Raleigh scattering which is inversely proportional to the forth power of wavelength. Mid IR fibers have potential applications in long-distance fiber optics communication systems since the predicted optical losses are 2-3 orders of magnitude less than those in fused quartz[9]. At present, all mid infrared fibers are non-communication related. Such fibers find applications in directing 10.6  $\mu\text{m}$  CO<sub>2</sub> laser radiation in surgical, industrial, radiometric, and spectroscopic systems.

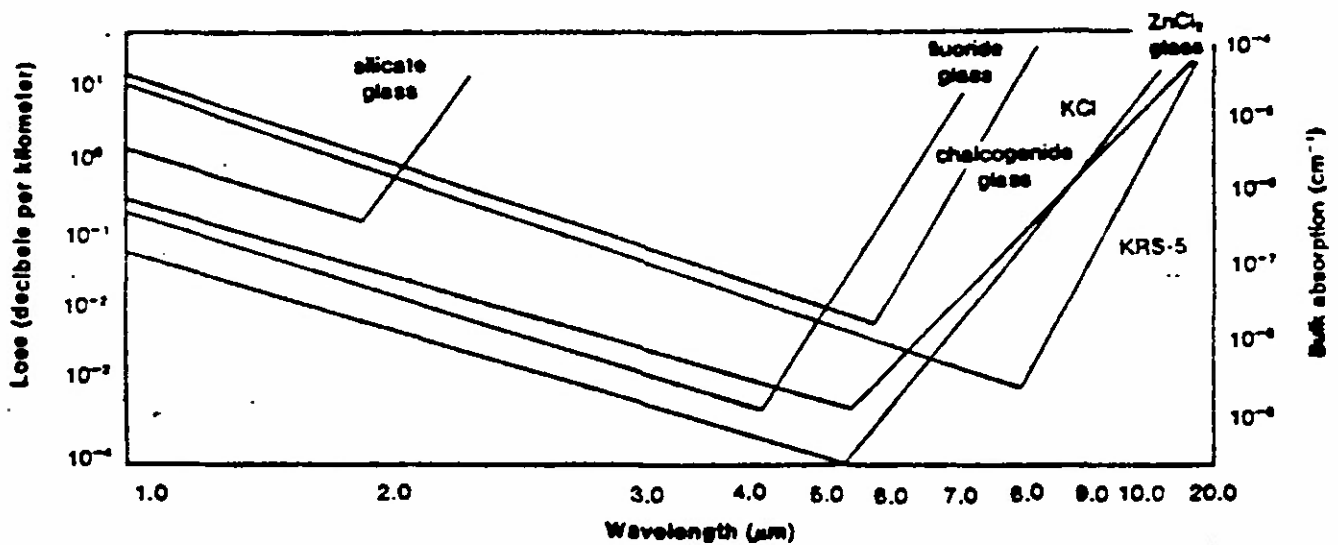


Figure 1.2: Theoretical minimum loss curves for infrared materials.

We have acquired three mid infrared fibers for the study of SBS phenomena. Two of these fibers are made of silver halide and the other is chalcogenide glass. KRS-5 fiber plays an important role in handling high-power delivery of laser beams and observation of SBS phenomena[4]. Because of its toxicity and brittleness, KRS-5 fibers had become obsolete when researchers have found more suitable materials, such as silver halide and chalcogenide and fluoride glasses, for handling high-power CO<sub>2</sub> laser. nevertheless, it is important to know the properties of KRS-5 fiber.

A: KRS-5 fiber

In crystalline materials, the region of low optical losses is bounded by the

1. Short-wavelength electronic absorption,  $\beta_e$
2. Long-wavelength multiphonon absorption,  $\beta_p$
3. SBS scattering loss,  $\Upsilon_B$

The intrinsic losses is the sum of the three losses:

$$\beta = \beta_e + \beta_p + \Upsilon_B \quad (1.13)$$

Table 1.4 shows the characteristic of optical losses in KRS-5 and KRS-6 crystals. At  $10.6 \mu\text{m}$  or  $943 \text{ cm}^{-1}$ , a simple calculation shows that for KRS-5 crystals,  $\Upsilon_B = 1.34 \times 10^{-3} \text{ dB/km}$ ,  $\beta_p = 3.74 \times 10^{-7} \text{ dB/km}$ , and  $\beta_e = 5.06 \times 10^{-11} \text{ dB/km}$ . This estimation shows the fact that SBS loss dominates the intrinsic absorption losses. Once extrinsic losses are removed, any nonlinear loss that occurs will be phonon related. Therefore, mid infrared fibers are very attractive mediums for the study of SBS phenomena.

Material	Short-wavelength Absorption Edge $\beta_e$	Long-wavelength Absorption Edge $\beta_p$	Brillouin Scattering Loss, $\Upsilon_B$
KRS-5	$5.3 \times 10^{-12} \exp(\omega/418)$	$9.0 \times 10^{-9} \exp(-\omega/25)$	$1.7 \times 10^{-18} \times \omega^4 \times n^8$
KRS-6	$1.1 \times 10^{-31} \exp(\omega/311)$	$4.7 \times 10^9 \exp(-\omega/43)$	$2.0 \times 10^{-18} \times \omega^4 \times n^8$

Note:  $\beta_e, \beta_p, \Upsilon_B$  in dB/km;  $\omega$  in  $\text{cm}^{-1}$

Table 1.4: Characteristics of optical losses in KRS-5 and KRS-6 crystals. After Dianov

The extrinsic losses are believed to be scattering due to crystalline impurities or imperfections and surface absorptions. The theoretical limits for the loss in KRS-5 crystals was predicted to be under  $0.1 \text{ dB/km}$  at  $10.6 \mu\text{m}$ . This promising feature has great potential in long-distance communication systems. Furthermore, the delivery of high power of up to  $100 \text{ W}$  in these fibers had been demonstrated[10]. Despite the above encouraging features, KRS-5 fiber has been plagued with toxicity, brittleness, and aging, which render it useless and unreliable in certain circumstances.

## B: Silver Halide Fiber

A more promising choice of suitable material for mid infrared fiber is the silver halide, particularly silver chloride and silver bromide of various compositions. Unlike KRS-5, the silver halide crystals are nontoxic, flexide and nonsoluble in water. The transmission loss of silver halide fibers manufactured by Sumitomo Electric Industries[11,12] is shown in Table 1.5. We have acquired two silver halide fibers for our experiment. The Sumitomo fiber is 1 meter long, a diameter of 700  $\mu\text{m}$ , and has a transmittance of 73.5%, which is equivalent to 1336 dB/km or  $0.308 \text{ m}^{-1}$ , according to the expression[13]

Fiber Composition		Transmission Loss at 10.6 $\mu\text{m}$
Core	Cladding	
100 wt % AgBr	Air	0.51 dB/m
99wt % AgBr-1 wt % AgCl	Air	0.39 dB/m
98wt % AgBr-2 wt % AgCl	Air	0.37 dB/m
100 wt % AgCl	Air	0.87 dB/m
100 wt % AgBr	100 wt % AgCl	0.22 dB/m

Table 1.5: Transmission loss of silver halide fibers [Sumitomo]

$$t(\%) = 100 \exp(-2\alpha\chi) = 100(10^{-\frac{\alpha\chi}{10}}) \quad (1.14)$$

where  $t$  is the transmittance, and  $\chi$  is the length of the fiber. The linear loss of a fiber can be found by using the cutback techniques and given as

$$2\alpha(\text{1/m}) = \frac{\ln(V_2/V_1)}{\chi_1 - \chi_2} \quad (1.15)$$

The conversion factor for  $\alpha(\text{dB/m})$  to  $2\alpha(\text{m}^{-1})$  is given by

$$a(\text{dB/m}) = \frac{10 \log(V_1/V_2)}{\lambda_1 - \lambda_2} = 4.34(2\alpha) \quad (1.16)$$

The other fiber is provided by Professor Katzir of Tel Aviv University in Israel. It has a diameter of 900  $\mu\text{m}$  and a length of 1.4 meter. The linear loss of this fiber can be approximately by fitting into the expression[14] depicted by Fig.1.3 as

$$a(\text{dB/km}) = 16.2\lambda^{-2} + 0.5 \quad (1.17)$$

At 10.6  $\mu\text{m}$ , the total loss would be 0.644 dB/m or 0.148  $\text{m}^{-1}$ .

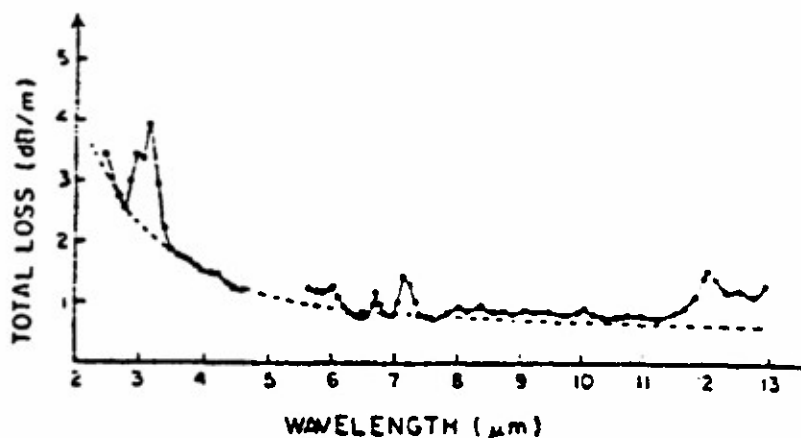


Figure 1.3: Total loss (dB/m) as a function of wavelength (solid line) in AgCl-Br fibers.

The effective interaction length of this fiber would be

$$L_e = \frac{1}{0.148} [1 - \exp(-0.148 \times 1.4)]$$

or 1.26 m. With a diameter of 900  $\mu\text{m}$  and assuming  $g = 0.075 \text{ cm/MW}$ , the threshold power is roughly 18.8 kW. The main disadvantage of using silver halide fiber is its sensitivity to UV light.

### C: Chalcogenide Fibers

Chalcogenide glass fibers of composition As-Ge-Se are transparent in the mid IR region. The theoretical minimum loss curve of a typical chalcogenide glass fiber is shown in Fig.1.2. From the curve, it is evident that these fibers have a minimum loss at a range of 5-6  $\mu\text{m}$ . Beyond this range, the loss increases. The present optical limitations of the chalcogenide glasses are related to extrinsic absorption losses associated with trace impurities such as oxygen, hydrogen and water.

Chalcogenide fibers find applications in the medical, industrial, and military sectors. Among those applications are remote IR sensing, imaging, remote IR spectroscopy, and laser beam guiding. We have acquired an unclad chalcogenide glass fiber from Infrared Fiber Systems, Inc for our experiments. The attenuation characteristic of this fiber is shown in Fig.1.4. The loss at 10.6  $\mu\text{m}$  is fairly high, i.e. about 8 dB/m. These fibers are very brittle compared to silver halide fibers.

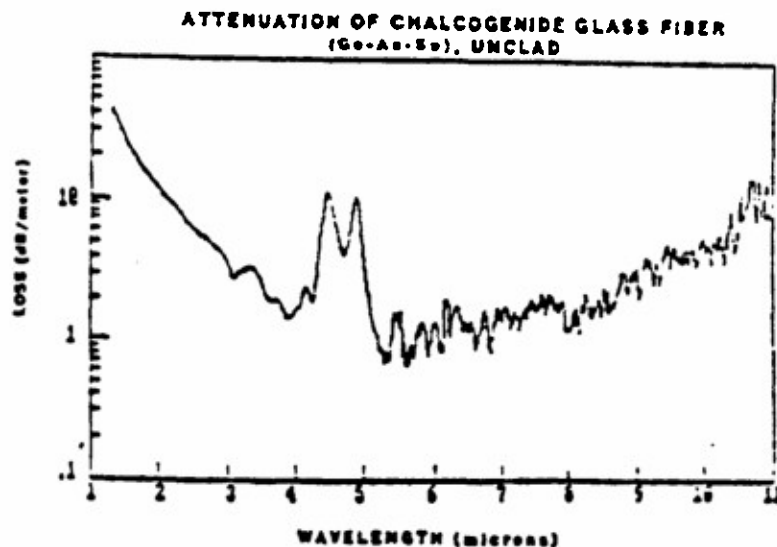


Figure 1.4: Attenuation of chalcogenide (Ge-As-Se, unclad) glass fiber [after Infrared Fiber System).

## 1.5 SBS in Infrared Fibers at 10.6 $\mu\text{m}$

The only two reported cases of SBS in mid IR fiber at 10.6  $\mu\text{m}$  were by Kovalev[4] and Yu[15], as was indicated in Table 1.1 of section 1.1. These two cases have a distinct similarity in the wave-shape of the reflected pulse, as shown in Fig.1.5 and 1.6. The intensity of the second peak is comparable to the incident pulse and detected at the trailing edge of the incident pulse. These features conform to the characteristic of SBS which reflects most of the power backward. The time delay associated with the second peak suggests that SBS has an inherent threshold to overcome. Another interesting feature is the periodic nature of the scattered signal as shown in Fig.1.5 and 1.6. Ippen explained that the buildup of the backward Brillouin wave results in a depletion of the pump wave near the input end of the fiber. This in turn reduces the gain in the fiber until the depletion region passes out of the fiber. The transit period of the resulting oscillation is expected to be  $2nL/c$ , where  $n$ ,  $L$ ,  $c$  are the index of refraction, length, and speed of light respectively.

Table 1.6 shows the various parameters involved in the excitation of SBS at 10.6  $\mu\text{m}$ . Unfortunately, the phonon lifetime and steady state gain coefficient of AgCl fiber is not available in any literature. In order to estimate the theoretical threshold for this fiber, we assumed a steady state gain value equal to that of KRS-5. With this approximation, a threshold of 17 kW was estimated. Our lower threshold, compared to Kovalev 48 kW, can be attributed to the longer fiber length and smaller diameter.

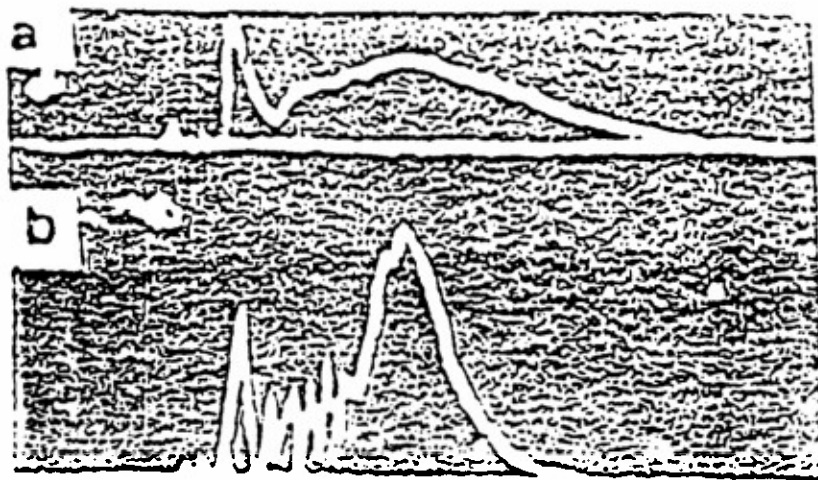


Figure 1.5: Waveform of (a) incident and (b) reflected pulse in KRS-5 fiber [Kovalev].

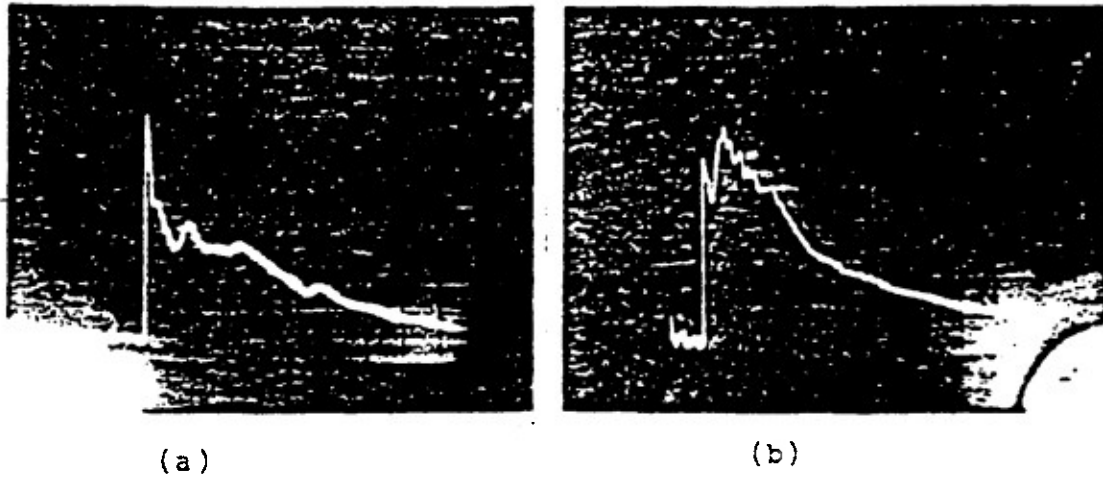


Figure 1.6: Waveform of (a) incident and (b) reflected pulse in Sumitomo fiber [Fong].

	Intensity (Mw/cm <sup>2</sup> )	Duration of Pulse ( $\mu$ s)	Linewidth $\Delta \nu$ (cm <sup>-1</sup> )	Phonon lifetime ( $\mu$ s)	Length (m)	Gain
Kovalev KRS-5	5.7	1 - 1.5	$4 \times 10^{-3}$ $2 \times 10^{-2}$	0.17	0.65	0.075
Yu AgCl	5.2	5	$5 \times 10^{-3}$ (150MHz)	-	1	-

Table 1.6: Comparison of various parameters for excitation of SBS at 10.6  $\mu$ m.

### 1.6 Typical Characteristic of SBS

It was mentioned earlier that SBS process is the dominant loss mechanism in long low-loss optical fibers because most of the power will be reflected backward, and the forward pump will be depleted. This phenomena[16] can be observed on a Fabry-Perot interferometer. Typical Fabry-Perot spectrum of the pump and reflected pulse is shown in Fig.1.7.

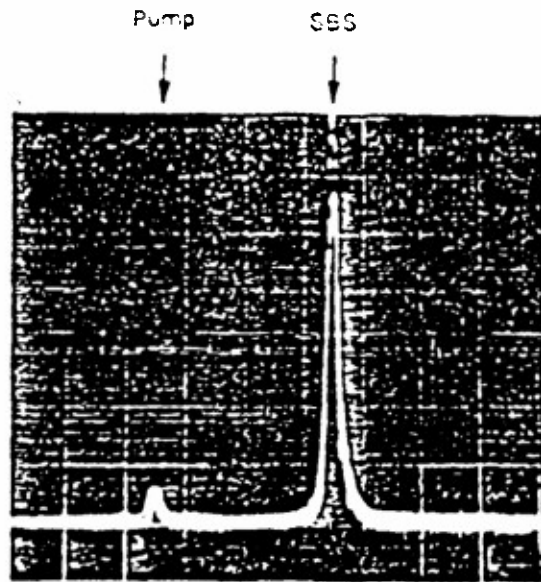


Figure 1.7: Typical Fabry-Perot spectrum of the backward light.

To illustrate the threshold of SBS, it is appropriate to plot the output power versus the launched power for the forward and backward light. Fig.1.8 shows the typical plot of output versus input power. At an input power lower than the threshold, the reflected power is mainly attributed to Fresnel reflection at the input end of the fiber. The transmitted power shows a linear increase as the input power increases. When the input power exceeds the threshold power, there is an exponential increase in the reflected power. Meanwhile, the forward light power no longer shows a linear increase but reaches saturation.

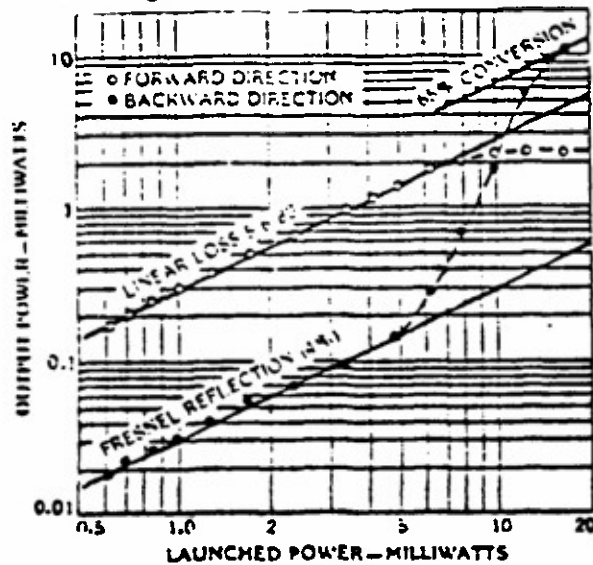


Figure 1.8: Transmitted and reflected power in SBS [after Cotter].

Another characteristic of SBS is the multiple frequency shifts due to scattering by acoustic wave. Stokes and anti-stokes wave of several orders may be observed in the forward wave as shown in Fig.1.9. The backward spectrum (B) is similar to Fig.1.7.

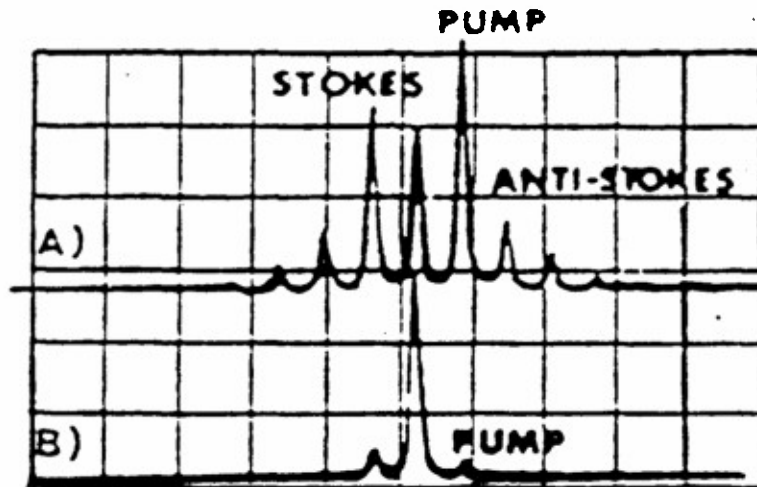


Figure 1.9: Output spectra of forward (A) and backward (B) light of a single mode fiber showing multiple-order stokes and anti-stokes scattering.

### 1.7 Proposed Experimental Setup to Observe Mode Patterns

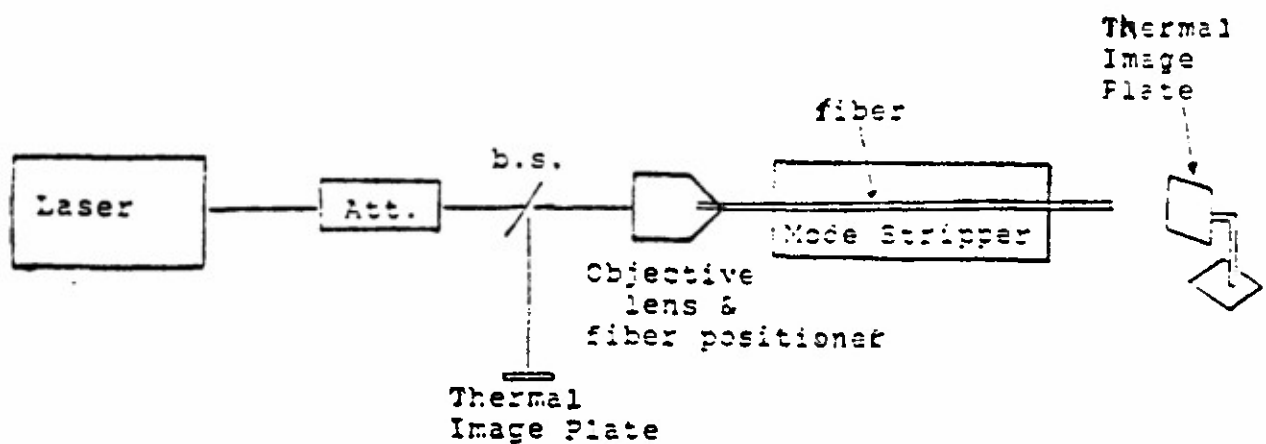


Figure 1.10: Proposed experimental setup to monitor mode patterns

A typical experimental setup to observe the mode patterns in an optical fiber is shown in Fig.1.10. Laser light is coupled into the fiber by means of the objective lens and the fiber positioner with x-y translational stage to alter the position and angle of the launched focussed laser beam. The variable attenuator serves to control the input power to the fiber so that the occurrence or non-occurrence of SBS can be conveniently chosen. The mode patterns of the transmitted pulse can be easily recorded with thermal image plates providing the near-field distribution. These patterns can be identified as pure LP modes, or a combination of two or more LP modes. The mode stripper, as has been pointed out earlier, is only needed for multimode fibers.

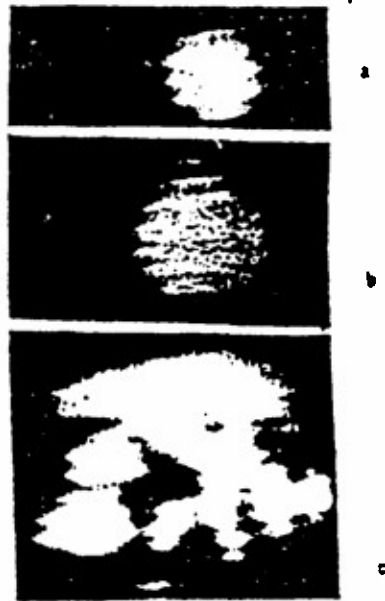


Figure 1.11: (a) backward SBS (b) incident, (c) transmitted wave pattern of a multimode fiber. After[17].

The typical photographs of the backward SBS wave, the laser radiation, and transmitted wave with  $P_i < P_{th}$ , are shown in Figs.1.11 (a), (b), and (c) respectively. The smaller spot size of the backward SBS wave is apparently related to the fact the nonlinear transfer of pump energy into the stokes wave proceeds with a low efficiency on the wings of the Gaussian beam. As expected, Fig.1.11 (c) illustrates the fuzzy pattern of the transmitted pulse with  $P_i < P_{th}$ . This pattern is related to the interference of different groups of modes with different phase velocities, which is a characteristic of a multimode fiber.

## 2.1 Introduction

– The intent of this experiment is to verify the possibility of modulating the laser pulse propagating in the fiber by means of external radiation that matches the acoustic frequency generated by the nonlinear Stimulated Brillouin Scattering process. SBS generated phonons as a result of electrostriction in the medium, form a diffraction grating which scatters the incident light. The interaction of photon and phonon results in either a forward or backward scattered photon or phonon. An external radiation injected into the system can conceivably interact through this nonlinear process. Hence, we have devised an experimental scheme to detect or boost phonon emissions by selecting a waveguide structure which is capable of guiding the external radiation to the fiber, as well as detecting any emissions and coupling it to the spectrum analyzer. The experimental setup is shown in Fig.2.1.

Before attempting to perform the experiment, we can estimate the low and high frequency phonons. To do so, we have to know the acoustic velocity in the medium. Unfortunately, this data is not available for silver chloride fiber. Therefore, the phonon frequencies were estimated using  $V_s = 2080$  m/s, which is the acoustic velocity of KRS-5 fiber at  $10.6 \mu\text{m}$ . A set of tuning curves for the low frequency phonon ranges from 1 to 5 MHz at  $10.6 \mu\text{m}$  for  $\Delta n$  varying from 0.005 to 0.025.  $\Delta n$  assumed a small value because the difference between the wavelength of forward scattered light and incident light is small. The set of low frequency phonon curves are shown in Fig.2.2. As for the high frequency phonon curves shown in Fig.2.3, it is evident that this frequency does not critically depend on  $\Delta n$ . At  $10.6 \mu\text{m}$ , the microwave phonon frequency is about 0.8 GHz. Therefore, the estimated range of phonon frequencies for both the forward and backward SBS is between the range of about 1 MHz to 1 GHz.

Improvements had been made to the waveguide that delivers the external radiation to the fiber. The waveguide used in previous experiments is certainly inadequate because of its dimension which cutoffs the propagation of the electromagnetic wave with the desired frequency. An attempt was made to construct a hollow waveguide with the correct

dimension such that the EM waves with frequency of at least 0.9 GHz will be allowed to propagate. In addition to hollow waveguides, the use of coaxial cables with embedded fiber in two configurations were also utilized in this experiment. These two configurations of the fiber in the coaxial cable will be presented in a later section.

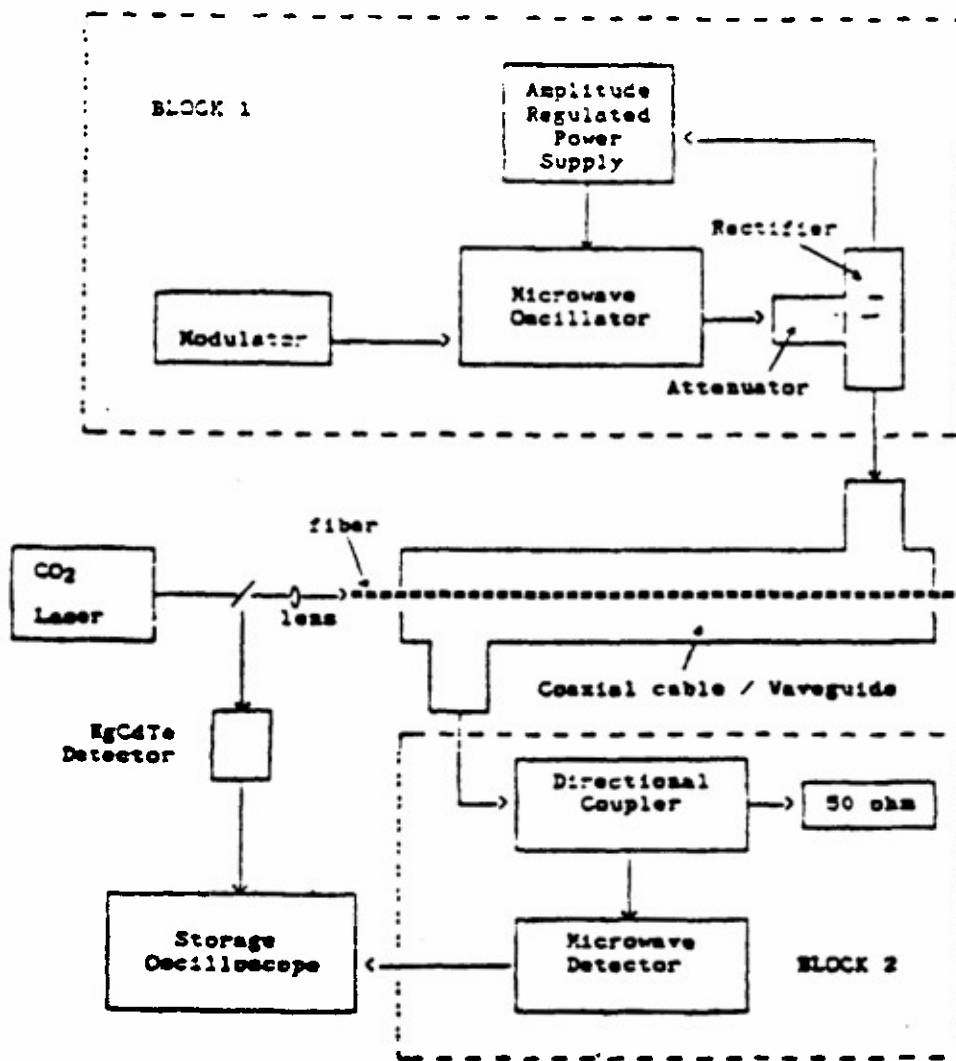
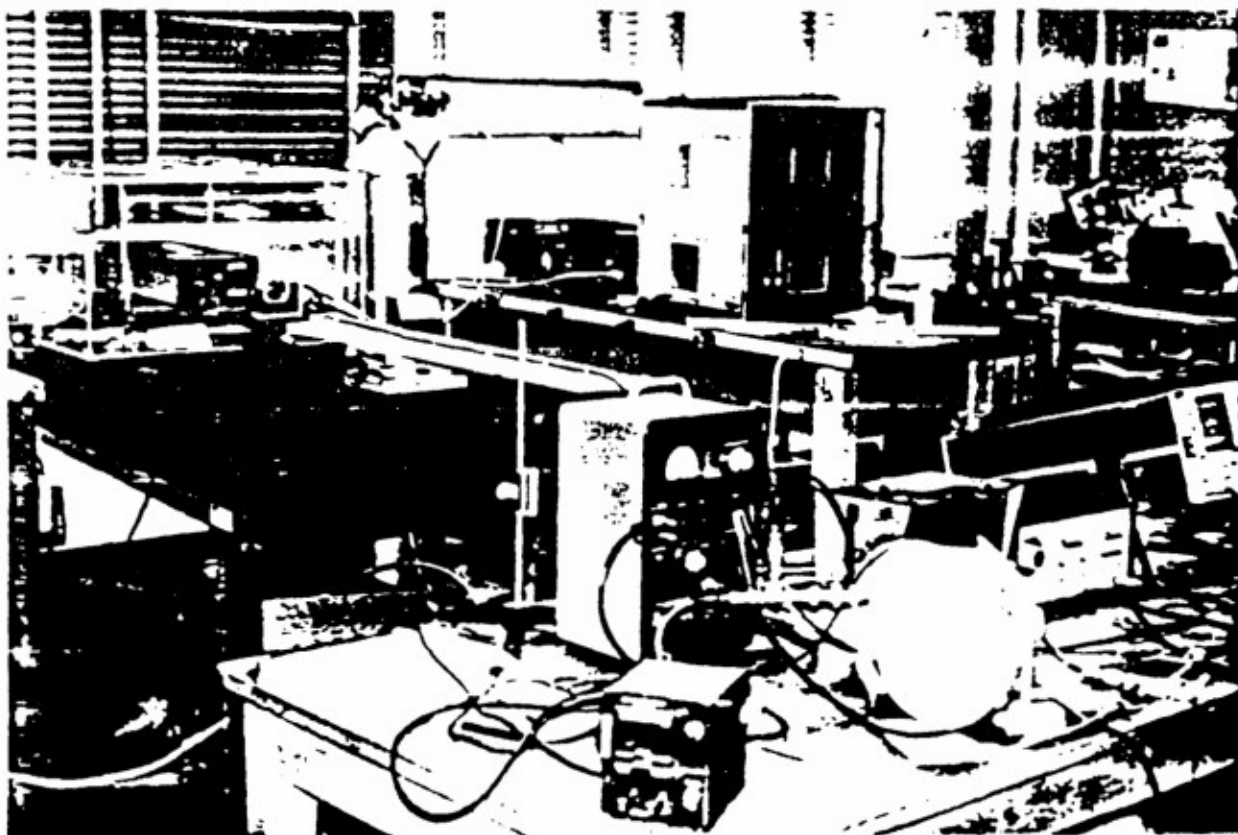


Figure 2.1: Schematic diagram of experimental setup



The detection of forward SBS spectrum in an optical fiber was reported by Shelby[18]. He estimated an acoustic-wave spectrum to be between 20 MHz and 800 MHz. He attributed this spectrum to thermal excitations in a fiber, which are eigenmodes of the cylindrical structure rather than the plane waves of the Brillouin theory. The acoustic-optic interaction takes place in a confined geometry that greatly weakens the usual Bragg condition. Therefore, he concluded that the scattered light spectrum consists of dozen of lines, each corresponding to a different cylindrical mode rather than the two lines of the Brillouin theory. An important lesson can be learned from Shelby's experiment. His experimental results proved that forward SBS is feasible in an optical fiber and the detected frequency shift is small. Since his operating wavelength is at  $0.647 \mu\text{m}$ , which is about 16 times less than  $10.6 \mu\text{m}$ , his estimation would correspond to a shift of 1 MHz to 50 MHz at the longer wavelength. Thus, our estimated low frequency phonons are not very far off from target. For resolving the forward stokes signal, Shelby resorted to Mach-Zehnder interferometer techniques.

The interaction of microwave with optical fibers reported by Auchterlonie[19,20] is another important verification that supports our hypothesis that light may be modulated by the interaction of the externally imposed electric field from the microwave signal with the dielectric material of the fiber. There is some similarity in his experimental setup, shown in Fig.2.4, and ours in Fig.2.1. The similarity is the irradiation of the fiber by microwaves. While the external radiation serves the same purpose, the arrangement of the fiber in the waveguide is different. We embedded the fiber between the two conductors of a coaxial cable, whereas Auchterlonie employed several configurations which include a single pass through a rectangular waveguide, a close wound coil, or a distributed coil of fiber placed inside the waveguide. Also, the vantage points are different. Our point of view favors the nonlinear interaction between the intense laser light and medium which alters the dielectric constant of the fiber. Their vantage point is primarily to reduce the change in dielectric constant by means of intense microwave energy, which is thermal in nature. Nevertheless, our goals are to achieve modulation of laser light in fiber by external means and to find new applications for this phenomena.

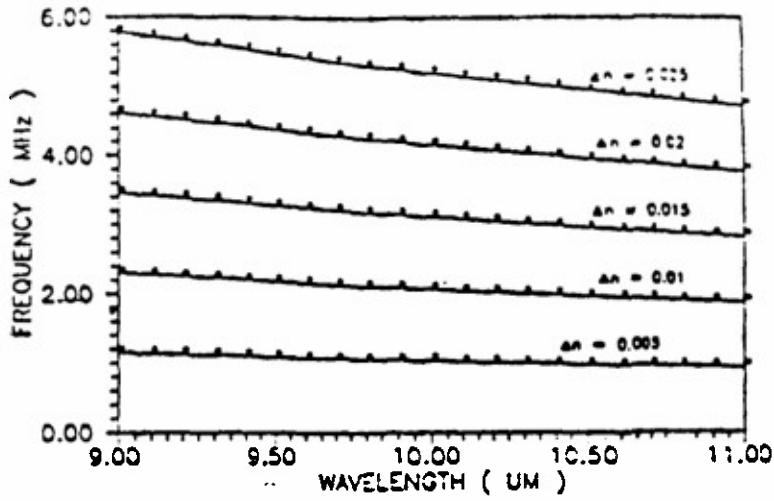


Figure 2.2: Low frequency phonon tuning curves

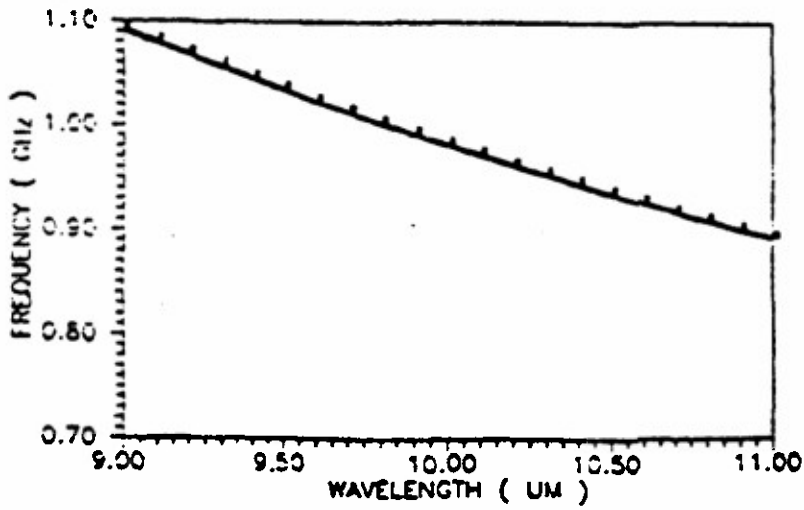


Figure 2.3: High frequency phonon tuning curves.

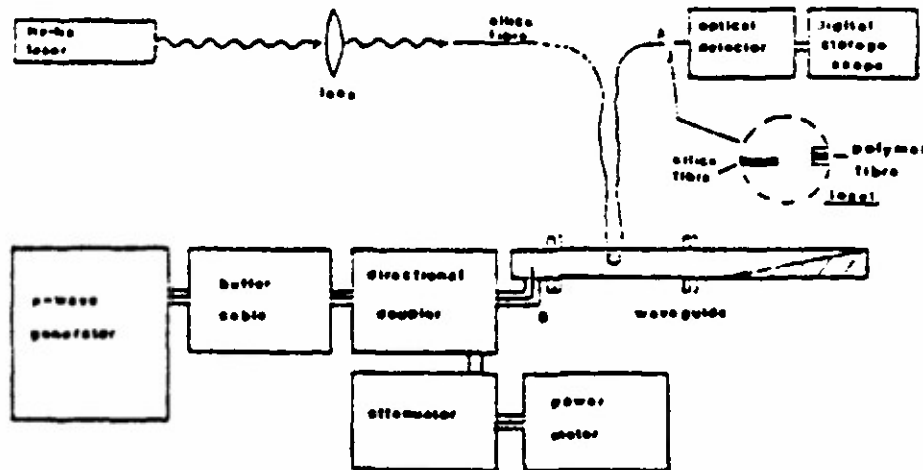


Figure 2.4: The experimental setup of microwave interaction with fiber. After[19].

## 2.2 Experimental Setup

The setup of our experiment is shown in Fig.2.1. Block 1 features the microwave generator system with a tunable oscillator having a range of 900 MHz to 2 GHz. This high power oscillator can provide the carrier frequency and modulating signal for a rf source. It is capable of AM modulation of the rf signal to facilitate detection by a square-law microwave detector. Before the microwave is delivered to the waveguide, it is attenuated and rectified. Part of the rectified signal is fed back to the amplitude-regulated power supply. This helps to ensure that the amplitude of the microwave signal is kept constant when the frequency is swept through its entire range.

Block 2 consists of the microwave detection system. The 50 ohm termination provides a matched load for the waveguide. It helps to ensure a travelling wave in the system rather than a standing wave. A travelling wave will provide a uniform interaction of the microwave and optical fiber. Block 1 and 2 are interchangeable to provide some flexibility to the launch directions of the microwave with respect to the laser pulse.

The waveguide system can be either a coaxial cable or a rectangular waveguide with the enclosed fiber in it. For a coaxial waveguide, the fiber is embedded between the two conductors of the cable. To do so, the cable is slit open a length of several inches shorter than the fiber. Then the outer strands of the conductor are partially removed to expose the insulated inner conductor. The next step is to slightly elevate the inner conductor so that a piece of aluminum foil can slip underneath it and in contact with the remaining outer strands of conductor. Then pressure is applied to the inner conductor so that it fits in the groove. Finally, the fiber is placed on top of the insulated inner conductor and wrapped around with the aluminum foil. The cross section of this configuration is shown in Fig.2.5 (a). Fig.2.5 (b) is another variation with the fiber placed next to the inner conductor, as

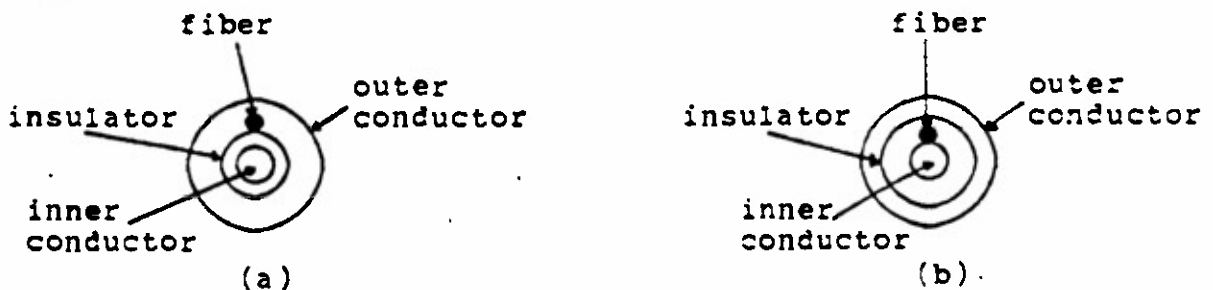


Figure 2.5: Cross section of coaxial cable with fiber inserted.

Other than coaxial cables, metallic rectangular waveguide can also be used. The rectangular waveguide dimension that is suitable to carry the dominant mode with frequency higher than 0.9 GHz can be estimated according to the following equation

$$f_c = \frac{c}{2\pi} \left[ \left( \frac{m\pi}{a} \right)^2 + \left( \frac{n\pi}{b} \right)^2 \right]^{\frac{1}{2}} \quad (2.1)$$

where m and n are the mode numbers, a and b are the width and height of the rectangular waveguide respectively. Waves with  $f > f_c$  will propagate unattenuated in the waveguide. For TE<sub>10</sub> mode, i.e. m=1 and n=0, and  $f_c=0.9$  GHz, the width of the waveguide should be at least 17 cm. Table 2.1 shows the five modes of lowest frequency with an air-filled rectangular waveguide with dimensions of 17 cm by 2.5 cm. A rectangular waveguide with the above dimension was constructed. From the table, it is clear that this waveguide is designed to carry the TE<sub>10</sub> and TE<sub>20</sub> mode for our applications.

Mode	m	n	$f_c$ (GHz)
TE <sub>10</sub>	1	0	0.9
TE <sub>20</sub>	2	0	1.8
TE <sub>01</sub>	0	1	6.0
TE <sub>11</sub> TM <sub>11</sub>	1	1	6.1

Table 2.1: The cutoff frequency for various modes in a rectangular waveguide of dimension 17 by 2.5 cm.

The laser source is a repetitive pulsed CO<sub>2</sub> laser with a 5 μs pulse and 90 mJ energy. It can deliver high-power and its radiation is strongly absorbed by human tissue, thus it is attractive for laser surgery. Besides medical usage, CO<sub>2</sub> laser is also attractive for the study of nonlinear phenomena in mid IR fibers, which has not been rigorously pursued by researches as compared to visible and near IR fibers. The most common problem lies with reliability introduced by vacuum seals, cathodes, and anodes, in addition to lifetime limitations because CO<sub>2</sub> chemically reacts with the gas discharge devices to form CO and broader gas laser linewidth. Another disadvantage is the requirement for cryogenically

cooled detectors. Our laser had been serviced once for a hairline crack in the discharge device.

The fibers available for this study are a silver halide fiber provided by Professor Katzir of Tel Aviv University, Israel, a chalcogenide fiber manufactured by Infrared Fiber Systems, and a silver halide fiber by Sumitomo.

### 2.3 Field Patterns in Waveguide

The hollow rectangular waveguide, by far, is the most commonly used waveguide structure and can support the TE and TM waves, but not TEM. There are several advantages of utilizing the dominant propagating mode. One of them is the independence of the cutoff frequency with the  $b$  dimension when the mode number  $n=0$ . Thus, a smaller  $b$  dimension of the waveguide can be designed just to carry the dominant mode and eliminating higher-order modes. More importantly, the other advantage is the feature of fixed polarization of the electric field in the transverse plane of the waveguide, as illustrated in Fig.2.6.

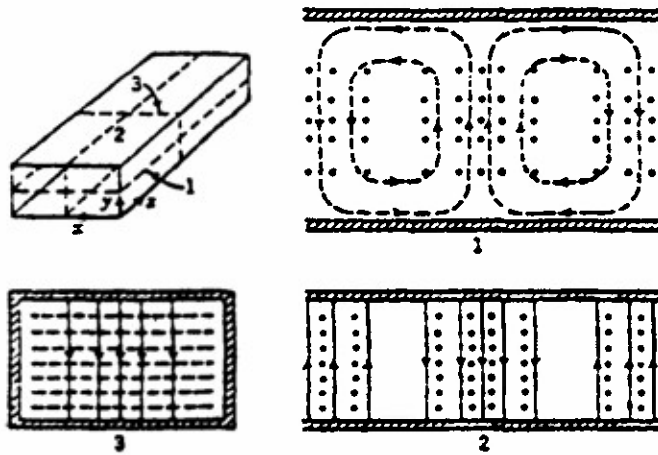


Figure 2.6: The field configuration of  $TE_{10}$  mode.

The E field strength of the  $TE_{10}$  mode is given by

$$E_y = E_0 \sin \frac{m\pi x}{a}$$

Thus, at  $x = a/2$ , the electric field strength will be a maximum at the center of the waveguide, and zero at the conducting walls. In view of this distribution of field strength, it is appropriate to place the fiber in the middle of the waveguide. Above 1.8 GHz, the second lowest mode,  $TE_{20}$ , will be allowed to propagate. However, the E field strength will be zero at  $x = a/2$ , but has maximum at  $x = a/4$  and  $x = 3a/4$ . Therefore, it may be necessary to adjust the position of the fiber in anticipation for this mode. The field distribution of the  $TE_{20}$  mode is shown in Fig.2.7.

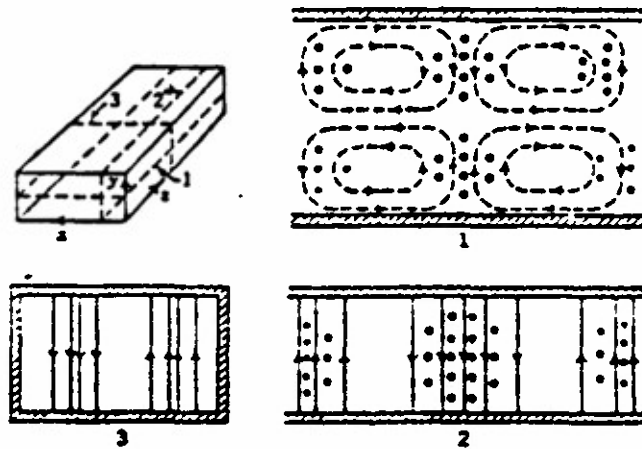


Figure 2.7: The field configuration for  $TE_{20}$  mode.

Coaxial lines are suitable for transmission from zero frequency up to about 10 GHz, although at this latter frequency attenuation restricts its use. The skin depth of a conductor is inversely proportional to the square-root of the frequency. Thus, higher frequencies correspond to shallow skin depth and small cross-sectional area, and therefore, the resistivity increases. Unlike rectangular waveguide, the coaxial cable can support the TEM mode, which is the principle mode of propagation. Another important mode is the  $TE_{11}$  mode which has the lowest cutoff frequency. The field configurations for various modes pertinent to the coaxial line[21] is shown in Fig.2.8.

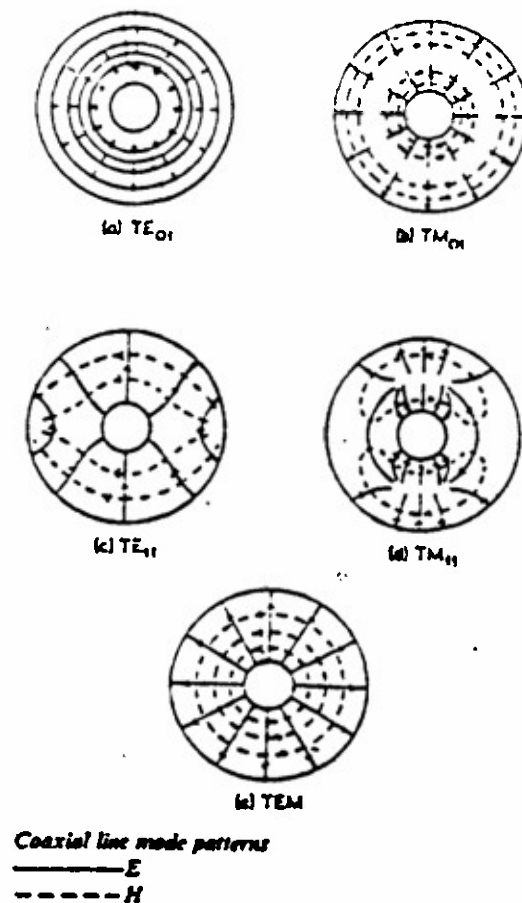


Figure 2.8: The field configurations of the coaxial line. After[21].

The interaction of the external guided EM waves with the fiber is difficult to analyze. For maximum interaction, the guided wave should have its E field parallel to that in the fiber. Due to the multimode nature of mid IR fiber, the mixture of modes in the fiber are ambiguous and leads to less effective interaction. The depolarization of the E field in optical fibers may also lead to inefficient interaction.

The "homemade" waveguide is not ideal with regard to compatibility with the theoretical mode patterns. Also, the open-end of the rectangular waveguide is detrimental to achieving a true travelling wave in the guide. Therefore, standing waves as a result of reflection by unmatched end, are dominant in this sort of experimental scheme. The fiber embedded coaxial cable, on the other hand, is also less than ideal because of "uneven" surfaces for the outer conductor, which is partially replaced with aluminum foil. The performance of these waveguides cannot be evaluated quantitatively, but, their experimental frequency responses will shed some light on their characteristics.

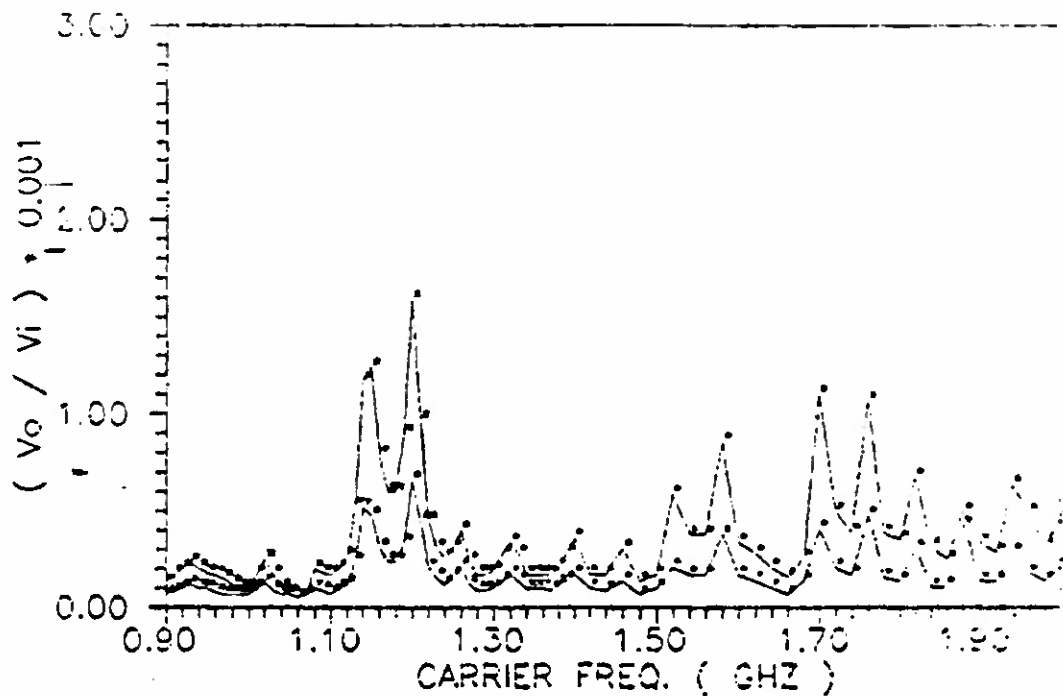


Figure 2.10: Transmission spectrum of 5 by 1.5 cm waveguide

## 2.4 Experimental Results

### 2.4.1 Frequency Response of Waveguide

The first stage of our experiment involves rigorous testing of the rectangular waveguides to determine their transmission spectra. One such waveguide used in Ref.[1] has a dimension of about 5 cm by 1.5 cm. It is evident that such dimension would not be feasible to deliver the microwave having the frequency range of 0.9 GHz to 2 GHz. In fact, the lowest  $TE_{10}$  mode would have a cutoff frequency of 3 GHz with this dimension. The transmission spectrum of this waveguide is shown in Fig.2.10. As expected, the signal arrived at the end of the waveguide is severely attenuated. Some frequency components are essentially cutoff. Furthermore, the detected wave may not be guided, but radiated because of the short length (2 feet) of the waveguide.

The waveguide structure that we have chosen to confine the microwave radiation to the fiber is a coaxial cable. This configuration allows for better coupling of microwave energy to the fiber than the hollow waveguide because of the higher field intensity confinement in a smaller area. The transmission spectrum of the coaxial cable and the better designed hollow rectangular waveguide is shown in Fig.2.11 and 2.12.

A matched load of 50 ohm was used as a termination load for the coaxial cable to eliminate reflection. As expected, the spectrum of Fig.2.11 shows a smoother response compared to Fig.2.12, which has no matching load. The spectrum of Fig.2.11 is more desirable in view of its almost flat response. It is also more lossy with the insertion of fiber, compared to the spectrum of the original cable shown on the upper curves of Fig.2.11. The newly acquired amplitude regulating power supply also helps to ensure the output of the microwave oscillator constant when the frequency is swept through its entire range.

#### 2.4.2 Phonon Detection

The second stage in our experiment involves the detection of phonon emissions. Block 2 of Fig.2.1 is replaced by a spectrum analyzer, which is capable of detecting rf and microwave frequencies. The coaxial waveguide is connected directly to the input of the spectrum analyzer. The laser is then turned on and its radiation is focused on the entrance end of the fiber. Under CO<sub>2</sub> pumping of the fiber, the spectrum is first tuned to the estimated range of low phonon frequencies (1 to 10 MHz). With the spectrum analyzer set to its most sensitive scale, the radiation pickup was carefully observed. A typical picture of such detected radiation is shown in Fig.2.13. The detected radiation which appeared in the fluorescence screen as "spikes" was not attributed to phonon emissions, but to electrical noise. Therefore, we could conclude that low and high phonon frequency emission were too weak or not observed with the Sumitomo, Katzir, and chalcogenide fiber.

This type of detection is very unreliable because the spectrum analyzer has to operate on a very sensitive scale, which allows noise or EM interference from other electronics devices to be picked up. The split cable approach also enhanced the pickup of unwanted radiation by the spectrum analyzer. Unless the emission is very strong compared to the electronic noise, there will always be a potential problem of misinterpreting the results.

Other means of detection and verification, such as the mode pattern approach, may be necessary.

### 2.4.3 Injection of External Radiation

— External radiation was injected into the system despite the failure to detect phonon emission. The reason is that we are doubtful as to whether the previously reported modulation was related to SBS or EM interference from other sources. The experiments were performed with external radiation delivered to the Katzir fiber in the hollow waveguide as well as the coaxial cable configuration. Interestingly, the "modulation" of the laser pulse by the rf frequencies of 0.2 MHz to 2 MHz reported by Fong was not attributed to SBS, but to the EM interference of the sources providing this radiation and the HgCdTe detector and its preamplifier unit. Such interference effects are shown in Fig.2.14 and 2.15.

The cause of this interference may be linked to unshielded wires that carry the power to the detector. Attempt was made to eliminate this problem by using shorter wires and a battery pack to drive the detector, but to no avail. It is quite impossible to completely shield the detector and its separate preamplifier unit because we have to leave the detector window unobscured. Perhaps, a better CO<sub>2</sub> detector with its window and amplifier in one shielded unit may be more suitable for our experiment. The HgCdTe detector has a major disadvantage because the preamplifier and the liquid nitrogen cooled detector are separate units. A shielded wire connecting the detector and preamp unit may introduce problem because the connection end of the detector is exposed and unshielded.

The GHz radiation was also introduced in the system. Any interference effect of this radiation on the detector will not be picked up because of the oscilloscope limitations. The transmitted pulse of Katzir fiber with injection of 1.3 GHz and 2 GHz are shown in Fig.2.16 and 2.17 respectively. Because the magnitude and pulse shape changes from pulse to pulse, it would be very difficult to infer from them any significant attributes of SBS phenomena as a direct result of the externally imposed radiation. Therefore, without a better laser with consistent pulse shape, the verification of this experiment would be impossible. Other means of detection with a beam profiler was attempted without much success. The main problem associated with this scheme of detection is the need of precise triggering mechanism to

synchronize the firing of the laser pulse with the profiler internal scan cycle. Also, the external trigger of the LP-30 laser is incompatible with our pulse generator because of the requirement of higher voltage of 10 V, rather than the normal 5 V TTL compatible pulse. The random detection of laser pulse without any synchronization was unsuccessful. Thus, the need for additional pulse generator and delay circuitry for proper synchronization place a budget constraint on our experiment. This scheme was later abandoned.

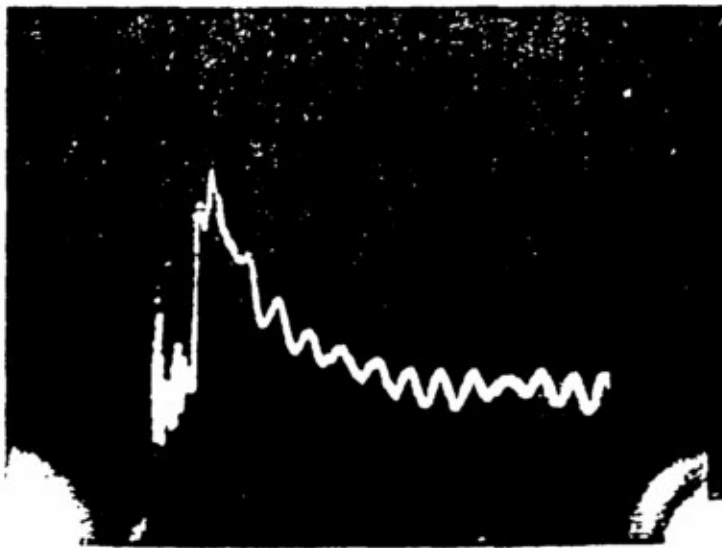


Figure 2.14: The interference effect of a 0.2 MHz radiation

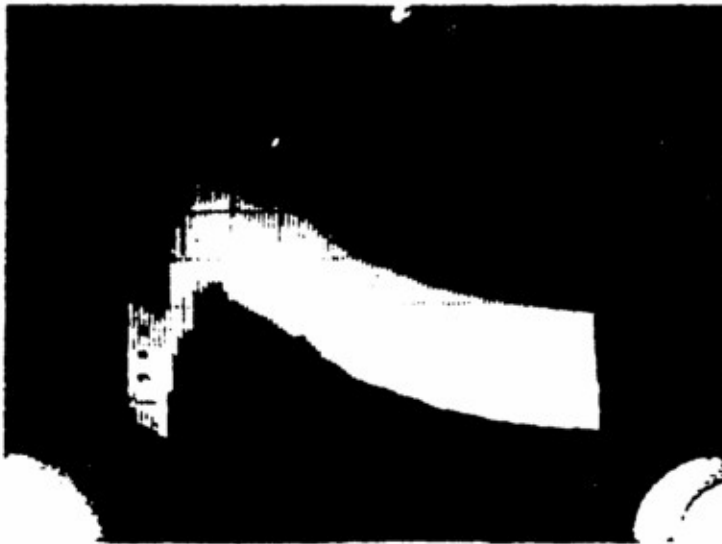


Figure 2.15: The interference of a 2.0 MHz radiation

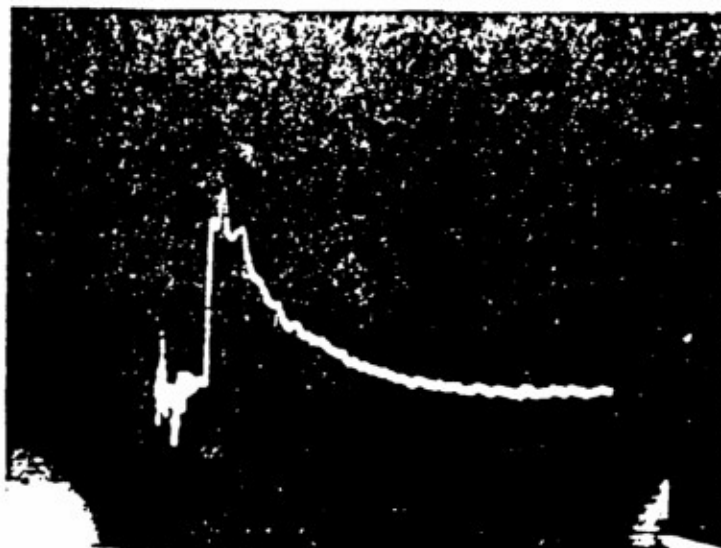


Figure 2.16: Transmitted pulse of Katzir fiber with 1.3 GHz radiation



Figure 2.17: Transmitted pulse of Katzir fiber with 2 GHz radiation

#### 2.4.4 Transmitted Pulse

The transmitted pulse can be detected with a high degree of certainty because the unwanted reflections can be conveniently blocked off. To do this, the detector is placed at the exit end of the fiber to monitor the transmitted pulse. A thick plastic slab, with a drilled hole holding the fiber, is placed in front of the detector to block off unwanted reflections from nearby objects. Thus, only the transmitted light emanating from the exit end will be detected. A sample of the transmitted pulse for the Sumitomo, Katzir, and chalcogenide glass fiber is shown in Fig.2.18 - 2.20 respectively.

On the contrary, the detection of the reflected pulse is not so easily accomplished without a beam splitter. Since the back reflection is a phase conjugate of the input wave, and traces the path of the input wave. Therefore, a beam splitter should be placed before the focussing optics if the reflected pulse is to be detected. Otherwise, secondary reflections from the entrance end of the fiber and the surrounding objects will overwhelm the detector. A typical experimental setup to monitor the backward wave is shown in Fig.2.21. note that the optical isolator was inserted between the laser and fiber to prevent the laser from being perturbed by feedbacks from the fiber. Without a mid IR beam splitter in our laboratory, the detected reflected pulse from the vicinity of the fiber entrance end will result in inaccurate measurement. Therefore, no attempt was made to monitor the reflected pulse.

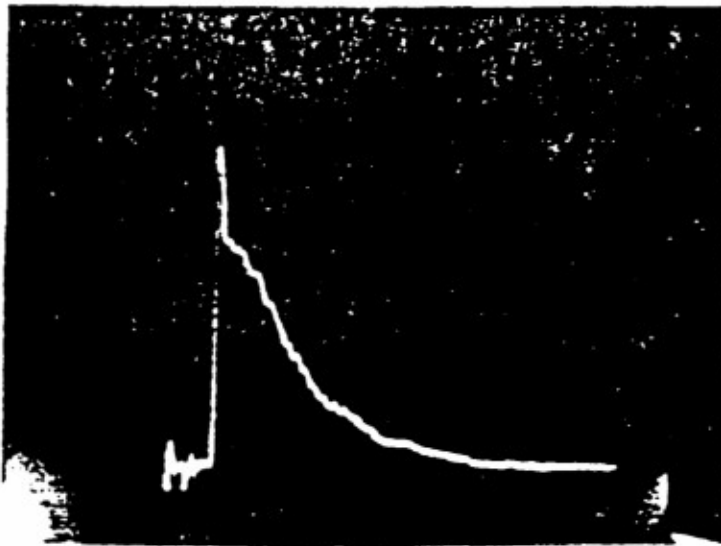


Figure 2.18: Transmitted pulse of Sumitomo fiber.

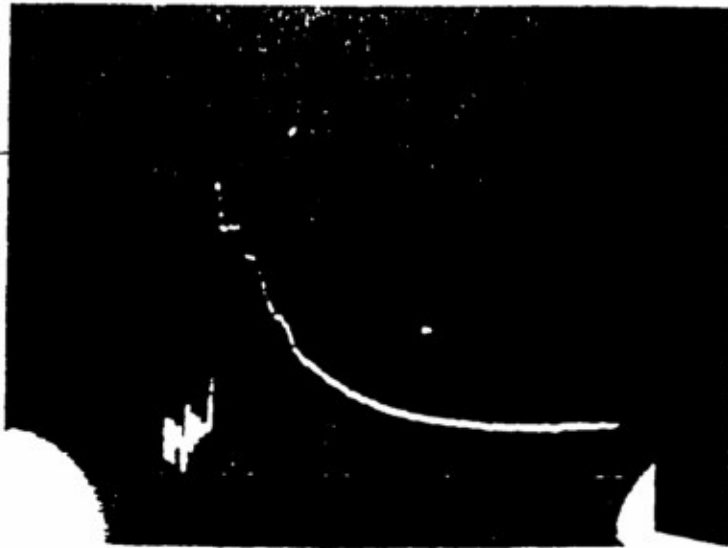


Figure 2.19: Transmitted pulse of Katzir fiber.

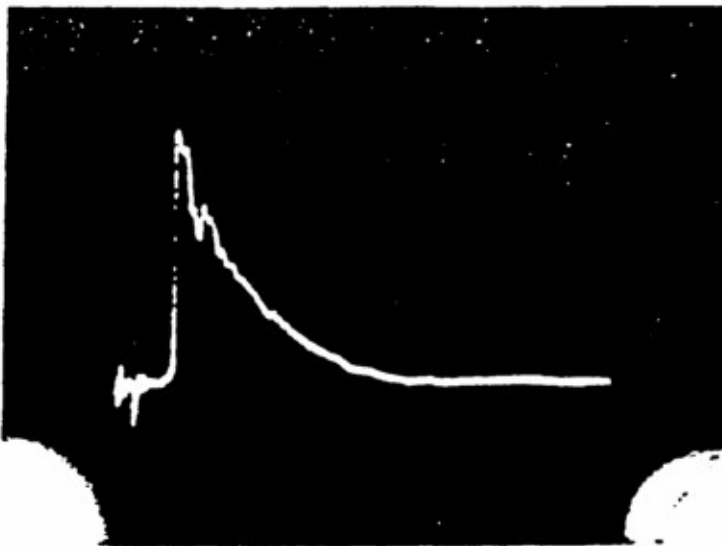


Figure 2.20: Transmitted pulse of chalcogenide fiber.

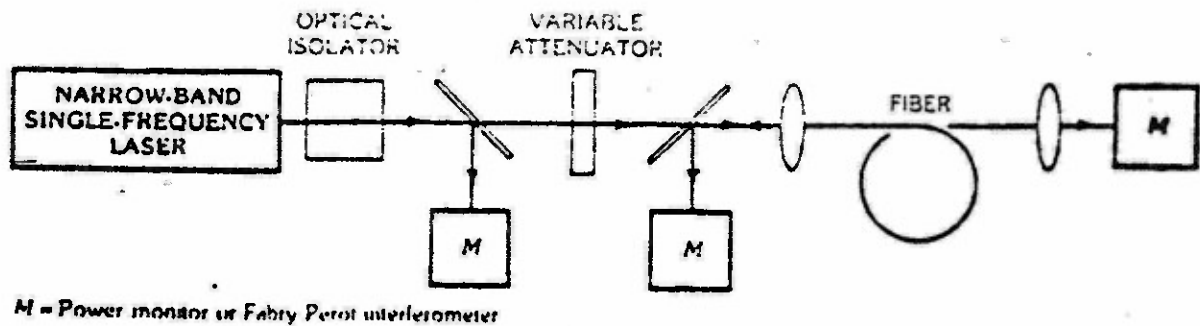


Figure 2.21: A typical experimental setup to monitor SBS at shorter wavelength.

## 2.5 Considerations for Improvements in Experimental Design

We have encountered significant difficulties in our techniques to observe and verify SBS phenomena in optical fibers at the mid IR range. Since our laser is not providing constant pulse shape and amplitude, it is impossible for us to evaluate the time domain pulse and infer any conclusions that may be significant to our study. There were attempts to monitor the spatial profile of the transmitted pulse with the Spiricon Beam Profiler, but without much success because of stringent requirements of synchronizing the firing of laser pulse with the Spiricon internal scan clock cycle. Additional hardware is needed for external triggering and synchronizing the laser pulse. This scheme is abandoned because of this obstacle. This approach is inexpensive, but certainly involved additional inconveniences, such as performing mode scrambling or cladding mode stripping on multimode fibers, unless single mode fibers are used.

Another area of improvement is the enhancement of microwave interaction with the fiber. Auchterlonie[19,20] had demonstrated that the primary and secondary coating of the fiber with acrylate and silver conducting paint respectively, will greatly enhance the absorption of microwave by the fiber. Besides coating, there are several configurations suggested by Ref [19] to achieve efficient absorption of microwave power. Such configurations with several passes, a close-wound coil, and a distributed coil of fiber in the

waveguide, are shown in Fig. 2.22 (a), (b) and (c) respectively. However, Ref [19] had not made a qualitative attempt to explain those configurations used, except to mention that the plane of the coiled fiber should be parallel to the electric field of the microwave.

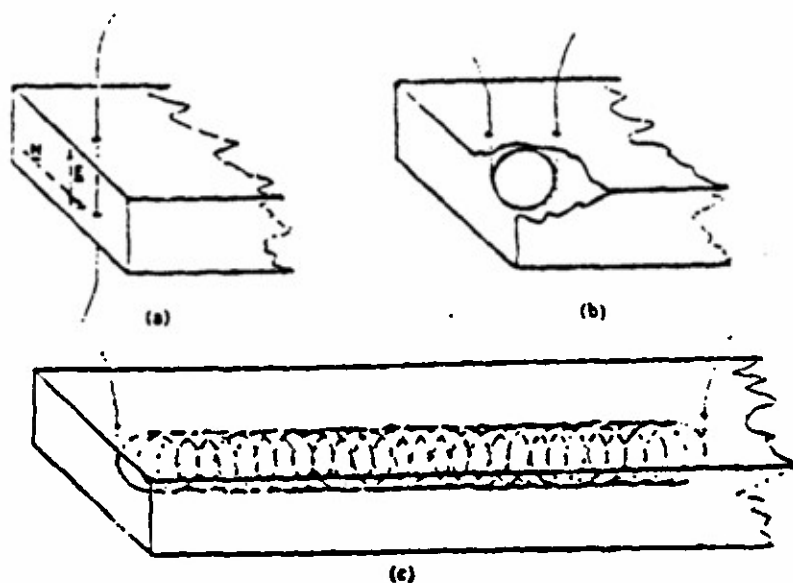


Figure 2.22: (a) Several passes of fiber, (b) A closed-wound coil, (c) A distributed coil of fiber in waveguide.

## CHAPTER 3 SWITCHING OF OPTICAL SIGNALS BY STIMULATED BRILLOUIN SCATTERING IN SINGLE-MODE OPTICAL FIBERS

### 3.1 Conventional Switches

Switching is a critical operation in communication and computing system. Switches function to reroute signals. Presently, the switches employed in optical systems are of the optoelectronic type[22]. With increasing demand of data communications, present optoelectronic switches cannot meet the requirements of optical fiber communications system due to their operational bandwidth, frequency range, etc.. If they can be replaced by all-optical switches, we can remove this main bottleneck and truly take advantage of the high-bit-rate provided by the optical fiber systems.

As optics has the capability of much higher frequency and much wider transmission bandwidth, together with high switching speed, low insertion loss, low crosstalk and high directivity, we can undoubtedly extend the total performance of the present optical systems greatly by the elimination of electronic control and manipulation in fiber-optic systems. Another advantage of all-optical elements is that the problem of excessive heating, due to reduction in size in electronics and proximity of conduction driven components, can be removed in optics. Usually excessive heating limits the electronic switching rate.

Recently, some researchers have arrived at the design of all-optical switch. It consists of a tiny segment of optical fiber, inside which are two distinct optical channels (waveguide). This fiber is formed out of a suitable nonlinear material. Based on this property, the light is switched by varying its intensity. This device can function at speeds of the order of  $10^{-12}$  second.

### 3.2 Theory of SBS Based All-optical Switches

We have for parametric interactions

$$\frac{dI_s(z)}{dz} = -gI_s(z)I_L(z)$$

$$\frac{dI_L(z)}{dz} = +gI_s(z)I_L(z)$$

$I_L$  and  $I_s$  are the intensities of incident and Stokes waves, respectively. According to Tang[23], the solution of the equations has the form

$$I_s(z) = \frac{I_s(0)[1 - I_s(0)/I_L(0)]}{e^{[1 - I_s(0)/I_L(0)]gI_L(0)z} - I_s(0)/I_L(0)} \quad (3.1)$$

$$I_L(z) = I_s(z) + I_L(0) - I_s(0) \quad (3.2)$$

We have for intensity ratio, at the fiber output end  $z=1$  to the input end  $z=0$ ,

$$\frac{I_L(l)}{I_L(0)} = \frac{I_s(l)}{I_L(0)} + 1 - k \quad (3.3)$$

$$\frac{I_s(l)}{I_L(0)} = \frac{k(1-k)}{e^{(1-k)G} - k} \quad (3.4)$$

Here, we let

$$k = I_s(0)/I_L(0) \quad (3.5)$$

$$G = I_L(0)gl \quad (3.6)$$

The family of curves of  $I_L(l)/I_L(0)$  versus  $I_s(l)/I_L(0)$  for various  $G$  is shown in Fig.3.1. It can be used to explain the properties of SBS based switches. We note that  $G \propto l$ , so that if  $G$  exceeds some threshold value, the SBS process arises from spontaneous scattering by thermal hypersonic vibrations, and the total pumping energy will stream to the second channel even in the absence of a pumping beam. According to Tang[23], the power spectral density of spontaneous Stokes wave for each mode is equal to

$$P_{sp} = k_B T \frac{c}{4\pi n^3 V_v} \quad (3.7)$$

where,  $k_B$  is the Boltzman constant,  $T$  is the temperature and  $V_v$  is the velocity of the wave

in the medium. For silica glass,  $V_v = 600$  m/sec, the Stokes bandwidth is 100 MHz[24]. From these parameters, the power of the spontaneous Stokes wave per mode of a fiber is of the order of  $10^{-9}$  W. For  $G = 20$ , the power of the amplified Stokes wave and the corresponding signal in the second channel will be  $\sim 0.5$  W, even in the absence of a driving beam. Thus, the amplification  $G$  should be set lower than 20. From Fig.3.1, if  $G=15$ , in order to switch 80% of the signal energy into the second channel, i.e.,  $I_1(l)/I_1(0)=0.2$ , the power of the driving beam should be equal to  $10^{-2}$  of the input power. To obtain an amplification  $G=15$  in a 10 m long single mode fiber with a core diameter of 5  $\mu\text{m}$ , the required incident power is about 2.5 W. (Assuming  $g = 5 \times 10^{-9}$  cm/W) and the driving power is about 2.5 mW.

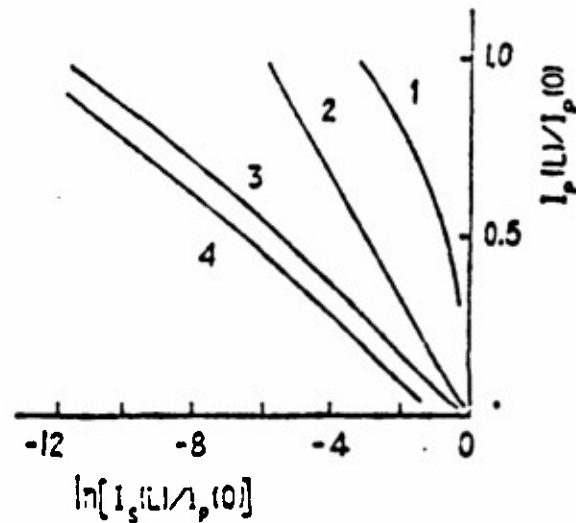


Figure 3.1: Dependence of Signal Intensity Switched to the First Channel on the pumping beam intensity:  $I_1(l)/I_1(0)$ -the ratio of the intensity switched to the first channel with respect to the input signal intensity; and  $\ln[I_p(l)/I_p(0)]$ -logarithmic ratio of the pumping beam intensity to the input signal intensity.

### 3.3 Design and Testing of a Prototype SBS-Based Switch

Based on this theoretical concept, the design of a prototype switch is shown as Fig.2.2 [22,25,26]. This switch operates in the following manner. A comparatively powerful signal with a wavelength  $\lambda_p$  (the signal radiation plays the role of the incident beam) is introduced through the beamsplitter 1 and lens 2 into the fiber 3. If the pumping beam is absent, the signal passes through the fiber without attenuation and into the first channel. When the pumping beam is introduced in channel 1 with the wavelength of  $\lambda_s$  (the Stokes wave), the nonlinear interaction between the incident and Stokes waves will produce the excitation of a hypersonic wave and energy exchange, transferring the energy of incident signal wave into the pumping wave. Thus the SBS process results in the switching of the signal from the first channel to the second. An experimental study on an SBS based switch is demonstrated as follows:

The materials needed to furnish this experiment:

1. Fiber 7 m long multimode fiber with a  $30 \mu\text{m}$  core diameter.
2. Incident wave 200 to 300 nsec pulses produced by a ruby laser with its power about 30W.
3. Stokes wave at the proper Stokes frequency with its power about 3 W.

**Experimental Procedure:**

**Step 1:** In the absence of the pumping wave. Let a signal wave of  $\lambda_p$  be introduced into the optical fiber.

**Phenomenon:**

The signal can be detected at the output without losses and enters the first channel, i.e. at  $\lambda_p$  wave range.

**Step 2:** The pumping wave of  $\lambda_s$ , the corresponding Stokes wavelength, is introduced, with the incident signal wave of  $\lambda_p$ .

**Phenomenon:**

About 70% of the signal power is detected at the  $\lambda_s$  wavelength, i.e. switching into the second channel.

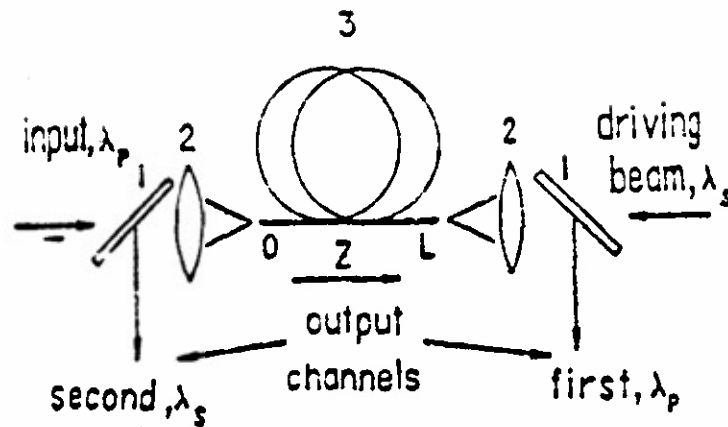


Figure 3.2: A SBS based prototype optical switch. Here, 1: beamsplitters, 2: focusing lenses and 3: a segment of optical fiber.

The main difficulty lies in the control of the frequency difference between these two waves. According to the momentum conservation law, the frequency of the Stokes wave should be less than the frequency of the incident wave by an amount equal to the acoustic wave frequency. However, this frequency difference is so small, usually, the difference is of  $10^{10}$  Hz, and the light frequency is of  $10^{16}$  Hz. High precision control of the Stokes frequency is essential.

### 3.4 Design of Implementable SBS Based Switch

Due to the difficult matching of the frequencies of these two waves, we try to generate the Stokes wave directly from the signal, instead of using another laser, lasing at the Stokes frequency. This experimental scheme is shown as Figs.3.3 and 3.5. This will greatly ease frequency matching of these two wave.

### 3.4.1 The Commercially Available SBS Based Optical Switch System

The incident beam at  $\lambda_1$  is split into three beams. The first is taken as the signal to be switched. The second impinges on a commercial Raman Shifter to generate the Stokes wave at wavelength  $\lambda_2$ . The third at  $\lambda_1$  is fed into commercial SRS Amplifier with the output from the Raman Shifter. The amplified wave at  $\lambda_1$  available with its power intensity above the SBS threshold is filtered and enters an SBS wave generator, which is commercially available as an SBS phase conjugator. Stokes wave at  $\lambda_2$  shifted from  $\lambda_1$  by acoustic phonon frequency is generated and is then fed into an attenuator before entering the SBS switch. The switch is controlled by the attenuator. If no switching is needed,  $\lambda_2$  wave is attenuated and since the switch is set below the threshold, the signal at  $\lambda_1$  will go through without the occurrence of SBS and enter Channel 1 shown on Fig.3.3; on other hand, when  $\lambda_2$  wave is not attenuated and therefore it enters the SBS switch above the SBS threshold, the signal at  $\lambda_1$  will be switched in the main channel to Channel 2.

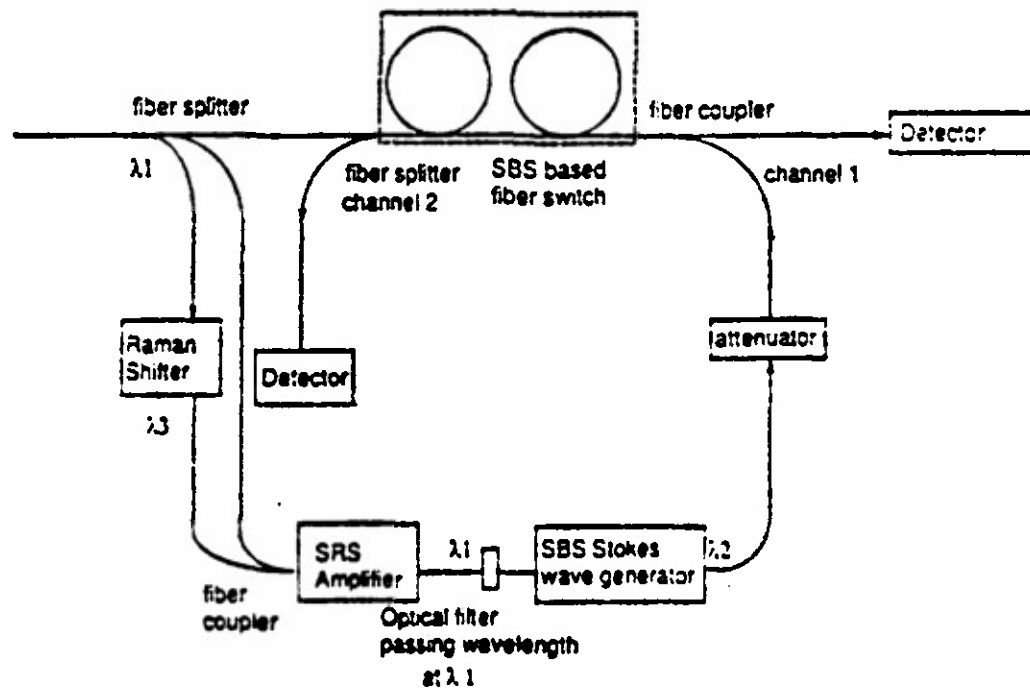


Figure 3.3: The SBS Based Optical Switch System Based on Commercial Components.

The Raman Shifter and SBS Stokes wave generator used in this experiment are, commercially available, such as the RS-101 RAMAN WAVELENGTH SHIFTER and PC-101 SBS PHASE CONJUGATOR MANUFACTURED BY PHOTON INTERACTION. The input-output wavelength of this Raman Shifter covers the range 1.064-1.54  $\mu\text{m}$  with different gases. The SBS Stokes wave generator is in the form of a phase conjugator, which reconstructs the pump waveform by a Stokes wave at  $\lambda_2$  with the SBS shift (in GHz). This unit serves our purpose as a Stokes wave generator at  $\lambda_2$ . Typically:

1. Phase conjugate reflectively  $\geq 70\%$ .
2. Input wavelength - 1.064  $\mu\text{m}$ .
3. Input beam reflective characteristics, shown on figure 3.4.

We note that all the commercial units used are not fiber-optic based.

### 3.4.2 The All Fiber-Based SBS Optical Switch System

In the above design, the fiber-optic link is broken at points, when the commercial units are used. This is a severe limitation, since it will render the system not EMI-proof. It is quite conceivable that an all fiber-optic based switch system is feasible. Figure 3.5 shows such an all fiber-optic switching system. This system is totally integrated and is thus EMI proof and should be highly efficient due to absence of any interfaces. We note that all the device functions are integrated into the fibers. Block B is the SBS amplifier, instead of SBS amplifier on Fig.3.3.

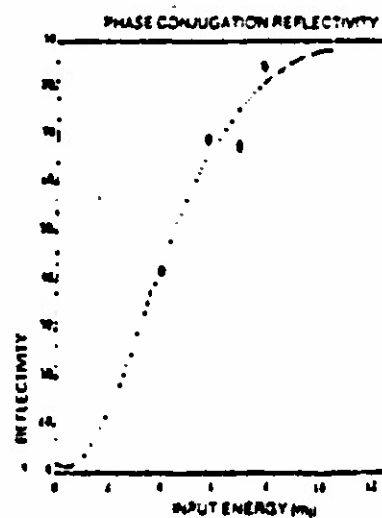
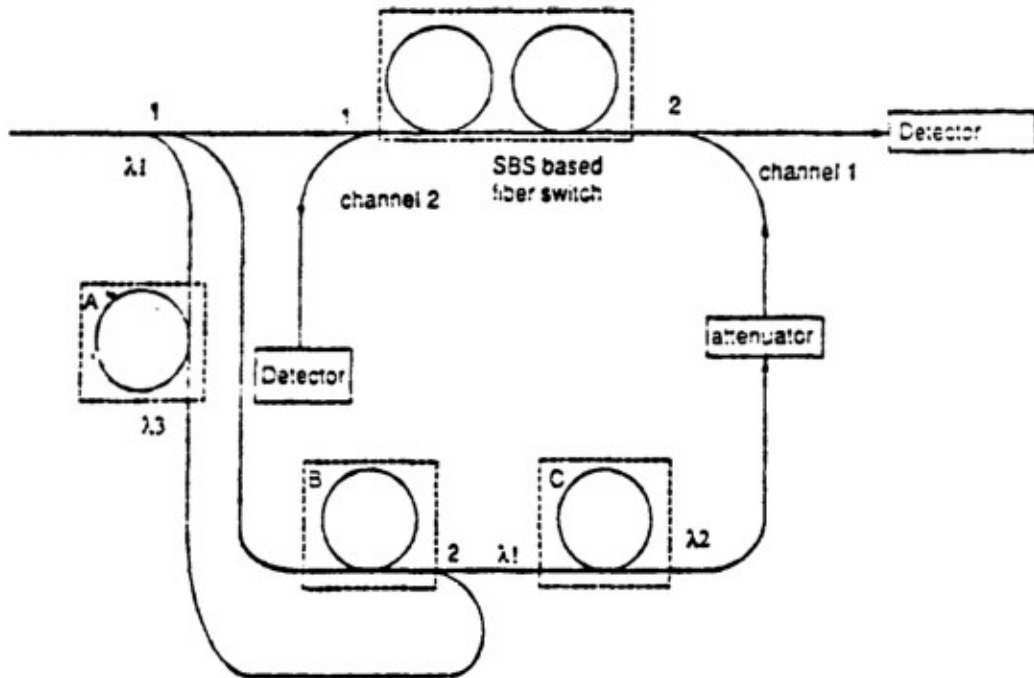


Figure 3.4: Input Beam Reflective Characteristic.



**Figure 3.5:** The all fiber-bounded SBS based optical switch system. 1: Fiber splitter; 2: Fiber coupler; A: SRS shifter; B: SBS Amplifier; C: SBS Stokes Wave.

## CHAPTER 4. PRELIMINARY STUDY OF FIBER RING FOR ENHANCEMENT OF SBS GENERATION IN MID IR FIBER

### 4.1 Introduction

— Stimulated Brillouin scattering (SBS) is a narrowband, low threshold nonlinear effect. It has been demonstrated that SBS can be used for optical demodulation, amplification and channel selection in densely packed wavelength division multiplexed system. However, its inherent small gain bandwidth product and high spontaneous noise have greatly limited its application.

There is a fiber configuration that is inherently noise suppressing, and that is the fiber ring[27,28]. Fig.4.1 gives an actual fiber ring setup.

In a high finesse, polarization maintaining optical fiber ring resonator, the threshold pump power for SBS generation is greatly reduced. Such reduction is due mainly to the ring resonator geometry that enhances significantly the circulating pump power, the ability of the fiber to ensure the identical polarization state of the pump and the scattered waves, thus maximizing the SBS gain coefficient, and the low loss nature of the device, necessitating only a few per cent round trip nonlinear gain.

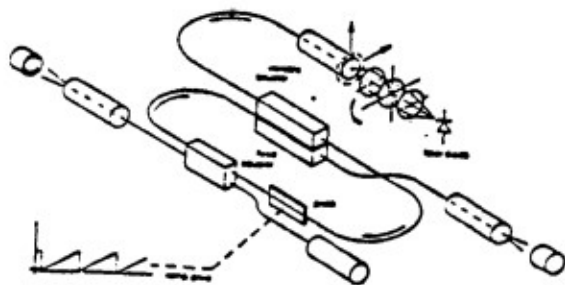


Fig. 4.1 Actual fiber ring setup

In propagating through the fiber loop, the pump wave is attenuated by the linear loss of the fiber and partially depleted by SBS scattering in the reverse direction. The linear loss also includes coupling losses at the couplers used to form the loop. The main advantage of the loop lies in the recurrent geometry, in which the backscattered SBS wave is repeatedly amplified by the incoming pump wave at the input port that is not attenuated by fiber loss and depleted by SBS, as opposed to the straight line structure in which the backscattered SBS signal encounters a progressively depleted forward traveling pump wave.

Practical success of the fiber ring in lowering the SBS threshold in low-loss fibers in the 1.3-1.5 $\mu\text{m}$  region to microwatt pump levels has also prompted us to consider the application of this technique to fiber based SBS studies in the 10.6 $\mu\text{m}$  region, where fiber attenuation is predicted to be orders lower than that in fused silica fibers.

#### 4.2. SBS ring in the near and mid IR

The anticipated lower theoretical loss and higher power handling capability of MIR fibers have been attracting research and development for communication, military and medical applications. They are increasingly being used as IR laser and information guided transmission, as well as in optical communication links with very low predicted transmission loss.

However, the extremely low loss of MIR fiber, being close to the Rayleigh scattering limit, undoubtedly results in the lowest Sbs threshold as compared to other nonlinear optical processes.

The principle of Sbs generation at 10.6 $\mu\text{m}$  is similar to that in the near infrared, and a comparison of the optical nonlinearities based on stimulated Brillouin scattering at 0.55-1.55 $\mu\text{m}$  and 10.6 $\mu\text{m}$  is given in Table 4.1.

It is noted that SBS gain at 10.6 $\mu\text{m}$  is about 10 times that at 1.55 $\mu\text{m}$ , because the metal halide fiber is phonon rich near 10.6 $\mu\text{m}$ . The observation of SBS at 10.6 $\mu\text{m}$  in a fiber waveguide made of KRS-5 has been reported, in which SBS threshold is approximately 85 kW.

Past extensive experimentation on our part [29] and by others in this spectral region

Table 4.1 Nonlinearities in 0.55-1.55 and 10.6  $\mu\text{m}$  region

Mechanism	Stimulated Brillouin scattering	
Process	Longrange acoustic phonon = pressure wave $\rightarrow$ change of optical susceptibility $\rightarrow$ pump scattering $\rightarrow$ generates Stokes shift wave	
Wavelength $\lambda$	Near infrared $< 2\mu\text{m}$	Mid infrared $10.6\ \mu\text{m}$
Equation of motion	$\omega_p = \omega_s + \omega_v$ $p$ = laser pump $s$ = Stokes $v$ = acoustic phonon	
Freq. shift $\nu$ Linewidth $\Delta\nu$	$\nu_B$ is narrow, $\approx 2nV/\lambda$ $\approx 11\ \text{Ghz}$ $V$ = velocity of longitudinal sound wave $\lambda$ = pump wavelength	$\approx 900\ \text{Mhz}$
Gain $g$	Backward direction only  $P_{12}$ = elasto optic coefficient $\rho$ = density Order of $10^{-11}\text{m/W}$	Order of $10^{-10}\text{m/W}$
$P_{\text{threshold}}$	$K=20$ For $\Delta\nu_p < \Delta\nu_B$ , order of $10^{-3}$ $W$ in long low loss fiber. Reduction by if $\Delta\nu_p > \Delta\nu_B$	Bulk : 85 kW  KRS-5 fiber: 20 kW  Fiber ring: 200 W

has met with limited success due to the lack of fibers with fiber attenuation comparable to that in current fused silica fibers at  $1.55\mu\text{m}$ , and single mode fiber of the metal halide variety is not yet in the market. All these factors contribute to high SBS threshold, making

Table 4.2 Fiber parameters

Fiber material	Silica			KRS-5
Wavelength ( $\mu\text{m}$ )	0.85	1.3	1.5	10.6
Number of mode	Single mode			Multimode
Brillouin gain $g_{\text{SBS}}$ $\times 10^{-11}(\text{m/W})$	4.2	4.5	4.5	75
Brillouin shift $\nu_B$ (Ghz)	20	13	11	0.9
Brillouin gain bandwidth $\Delta\nu_B$ (Mhz)	50	23	16	
Fiber loss (dB/km)	3	0.5	0.1	$1.3 \times 10^3$
Fiber core refractive index $n$	1.46	1.45	1.44	2.37
Effective area $A \times 10^{-11}(\text{m}^2)$	1.5	6	7.5	$7.85 \times 10^4$
Coupler loss	1%(0.05dB)			1dB

observation of the SBS phenomenon a rare occurrence. The success of SBS fiber ring in 0.5-1.5  $\mu\text{m}$  region prompts us to apply the fiber ring concept to this wavelength region, knowing that we will still be confronted with high fiber attenuation in the near future. The short ring length involved in the ring structure will eliminate fiber attenuation as a determining factor in the SBS generation threshold. Therefore, we are extending the model from 1.55 $\mu\text{m}$  to 10.6 $\mu\text{m}$ . The basic parameters are listed in Table 4.2.

#### 4.3. Evaluation of performance parameters of SBS fiber ring

A model is presented for analysis and emulation of the SBS generation that takes pump depletion into account and predicts the steady state threshold lasing power, optimum conversion efficiency, and saturation regime in terms of the ring parameters. A schematic diagram of an all fiber ring is shown in Fig.4.2.

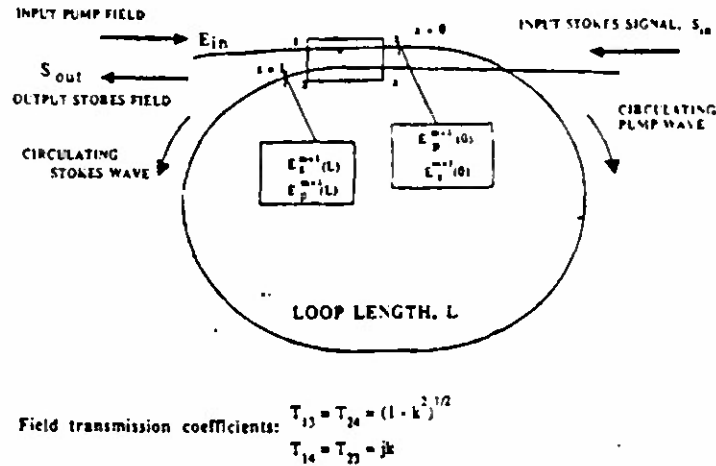


Fig.4.2 Schematic diagram of a fiber ring

The coupled equations describing the variation of the intensity of the pump and Stokes wave in a length of optical fiber are

$$dI_p(z)/dz = -g_B I_p(z) I_s(z) / A_{eff} - 2\alpha_0 I_p(z), \quad (4.1)$$

$$dI_s(z)/dz = -g_B I_p(z) I_s(z) / A_{eff} + 2\alpha_0 I_s(z) \quad (4.2)$$

where

- $I_p$ : pump intensity
- $I_s$ : Stokes wave intensity
- $2\alpha_0$ : linear attenuation coefficient
- $g_B$ : peak Brillouin gain coefficient
- $A_{eff}$ : effective area

For a typical fiber ring that has a short loop length ( $< 10$  m), the total Brillouin gain over one loop transit is small. Therefore the expression for the pump and Stokes intensity

transmission coefficient in the loop,  $T_L^2$ , can be obtained by integration of Eq.(4.1) and (4.2), respectively, yielding

$$I_p(L)/I_p(0) = T_L^2 = e^{-[2\alpha_0 + g_B I_s(0)]L} \quad (4.3)$$

$$I_s(L)/I_s(0) = T_s^2 = e^{[2\gamma_0 - g_B I_p(0)]L} \quad (4.4)$$

By considering propagation of the pump and Stokes fields around the ring loop, it can be seen that in the steady state

$$E_s(L) = jk(1 - 2\gamma)^{1/2} E_s(0) \quad (4.5)$$

where

$E_s$ : circulating Stokes field

$2\gamma$ : coupler intensity loss

$k$ : field coupling coefficient

By combining Eq.(4.4) and (4.5), we have

$$k^2(1 - 2\gamma)e^{[-2\alpha_0 + g_B I_p(0)]L} = 1 \quad (4.6)$$

This equation represents the familiar threshold condition for stimulated Brillouin oscillation when the loss-gain product is unity. Approximating  $k^2 \approx 1$ , the threshold pump intensity circulating in the loop can be derived:

$$I_p(0) = I_p = 2[(\alpha_0 + \alpha_k)L + \gamma]A_{eff}/g_B L \quad (4.7)$$

For a resonant situation the output at port 4 (see Fig.4.2) should vanish, therefore it can be shown that

$$I_p = I_s \frac{(1 - 2\gamma)(1 - k^2)}{[1 - k(1 - \gamma)T_L]^2} \quad (4.8)$$

By combining Eq.(4.7),(4.8), and (4.3), we obtain the expression for the output Stokes intensity,

$$I_{S,out} = T_{out} I_p (\sqrt{I_i/I_0} - 1) \quad (4.9)$$

where

$$T_{out} = (1 - 2\gamma)(1 - k^2) \quad (4.10)$$

$$I_0 = \frac{[(\alpha_0 + \alpha_k)L_\gamma]^3 A_{eff}}{[(1 - 2\gamma)\alpha_k g_B L^2]} \quad (4.11)$$

We can then define the conversion efficiency of the Brillouin laser as

$$\eta = \frac{I_{S,out}}{I_i} = T_{out} I_p \left( \frac{1}{\sqrt{I_0 I_i}} - \frac{1}{I_i} \right) \quad (4.12)$$

Differentiating Eq.(4.12) with respect to  $I_i$ , we find that the maximum conversion efficiency  $\eta_{max}$  is obtained when  $I_i = 4I_0$ , and

$$\eta_{max} = \left[ \frac{(1 - 2\gamma)(\alpha_k L)}{(\alpha_k L + \alpha_0 L + \gamma)} \right]^2 \quad (4.13)$$

Physically, this represents complete conversion of the circulating pump power above threshold into the Stokes power and represents gain saturation. From Eq.(4.9) and (4.13), it is clear that the performance of the fiber ring is determined by the specifications of the fiber, such as loss  $\alpha_0$ , effective area  $A_{eff}$ , and loop length  $L$ , and those of the coupler, such as coupler loss  $\eta$  and coupling coefficient  $k^2$ .

#### 4.4. SIMULATION RESULTS

Using the established module based on above analysis, a simulating program is

programmed with IDL (Interactive Data Language) which can be debugged and run under VAX/VMS operation system. Following figures will show the results of calculation with the parameters of fiber ring at 1.55-10.6 $\mu\text{m}$  region listed in Table 4.2.

First, consider the effect of the parameters of fiber and fiber ring on the performance of the ring in 1.55 $\mu\text{m}$ . Different coupling coefficient  $k^2$  are used, Figure 4.3 illustrates that undercoupling ( $k^2 < k_{res}^2$ ) can increase conversion efficiency at the expense of an increased SBS threshold. Fiber loss appears not to be a factor on ring performance (see Fig.4.4), because loop length is shorter than 10m. It hence is the basis of application of the ring technique to the 10.6 $\mu\text{m}$  region, where currently available fiber has high loss, 1dB/m.

From 10.6  $\mu\text{m}$  data, Fig.4.5 show that the technique of coupler fabrication play an important part in fiber ring reduction of SBS threshold, which is currently a bottleneck of 10.6  $\mu\text{m}$  fiber device. We can hopefully achieve higher conversion efficiency if improvement of fabrication technique for coupler at 10.6 $\mu\text{m}$  is implemented. It is very clear in Fig.4.5(a) an amazing reduction of  $P_{th}$  can be obtained in the case of the ring at 10.6 $\mu\text{m}$  with a reduction of  $P_{th}$  by 100 times to 200W in the case of the ring at 10.6  $\mu\text{m}$  with current available fiber, although larger effective area and higher loss lead to higher SBS pump threshold in a linear fiber. It makes possible the study of optical fiber nonlinearities at 10  $\mu\text{m}$ .

If the loss of fiber and coupler in the mid infrared achieves the level of current fused silics fiber at 1.55  $\mu\text{m}$ , the SBS threshold in the fiber ring will be as low as 7 $\mu\text{W}$  (see Fig.4.6). In the ideal low loss region at 10.6 $\mu\text{m}$  (see Fig.4.7) the ring device is significantly superior to similar device at 1.55 $\mu\text{m}$ , as demonstrated by an SBS threshold of less than 1 $\mu\text{W}$ , hence lower noise.

In summary, using the model that takes into account pump depletion, the analysis of fiber ring operating at 1.55 $\mu\text{m}$  is extended to 10.6 $\mu\text{m}$ . It is shown that the structure of the fiber ring can greatly reduce the SBS threshold at 10.6 $\mu\text{m}$  so that it would become possible to observe SBS at 10.6 $\mu\text{m}$  with lower pump power with presently available metal halide fibers. The results of simulation are included in the Table 4.3, Table4.4.

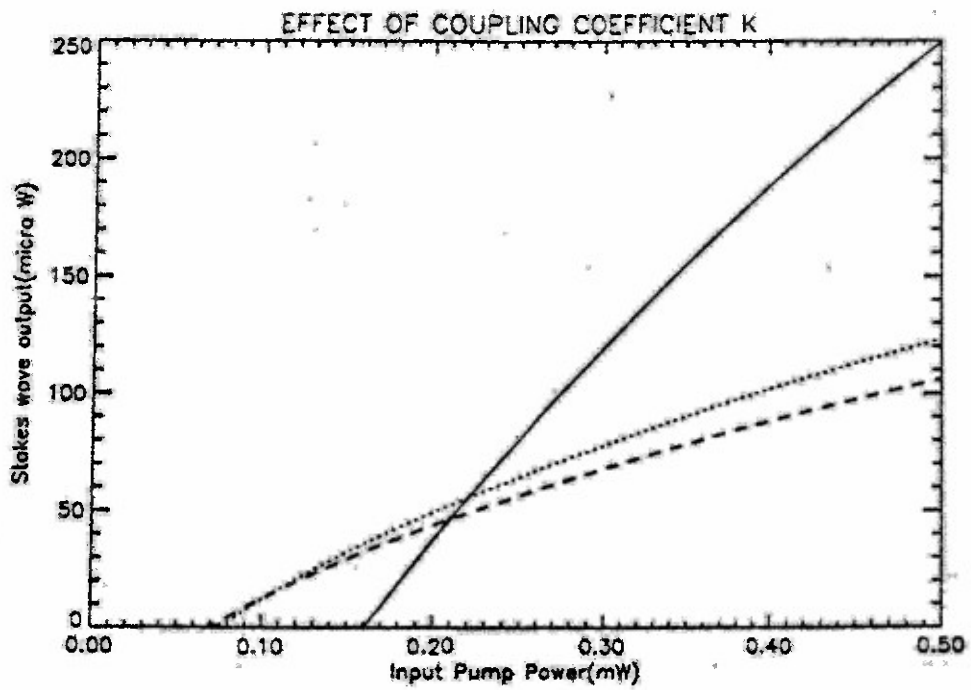
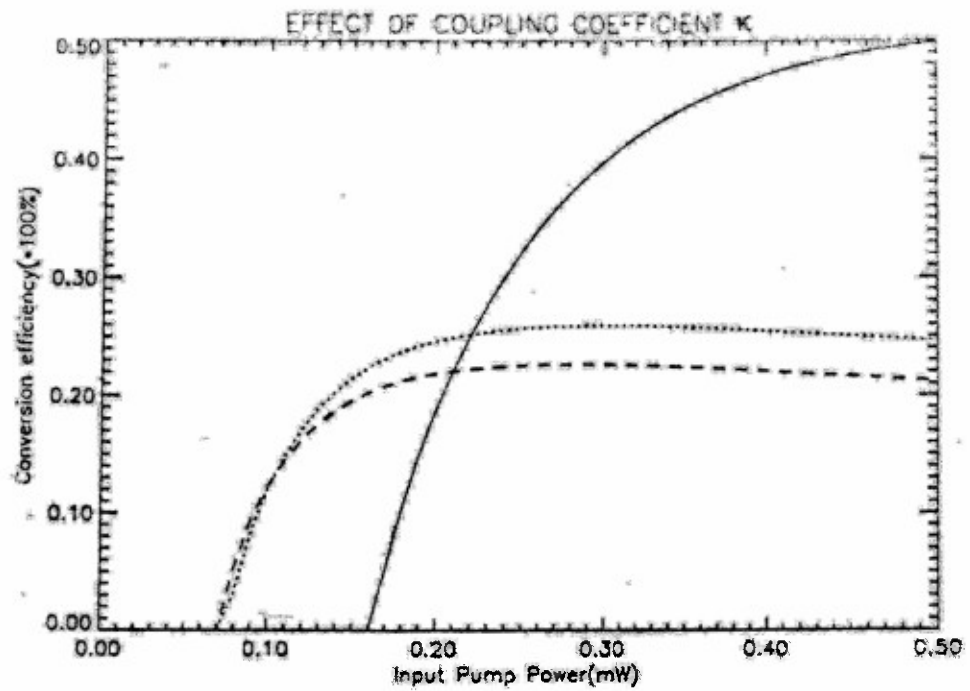


Fig.4.3 (a) Output Stokes power, (b) Conversion efficiency versus the input pump, with varying coupling coefficient  $k_2$ , at  $1.55\mu\text{m}$ , —  $k^2=0.9750$ , ...  $k^2=0.9897$ , -  $k^2=0.9910$

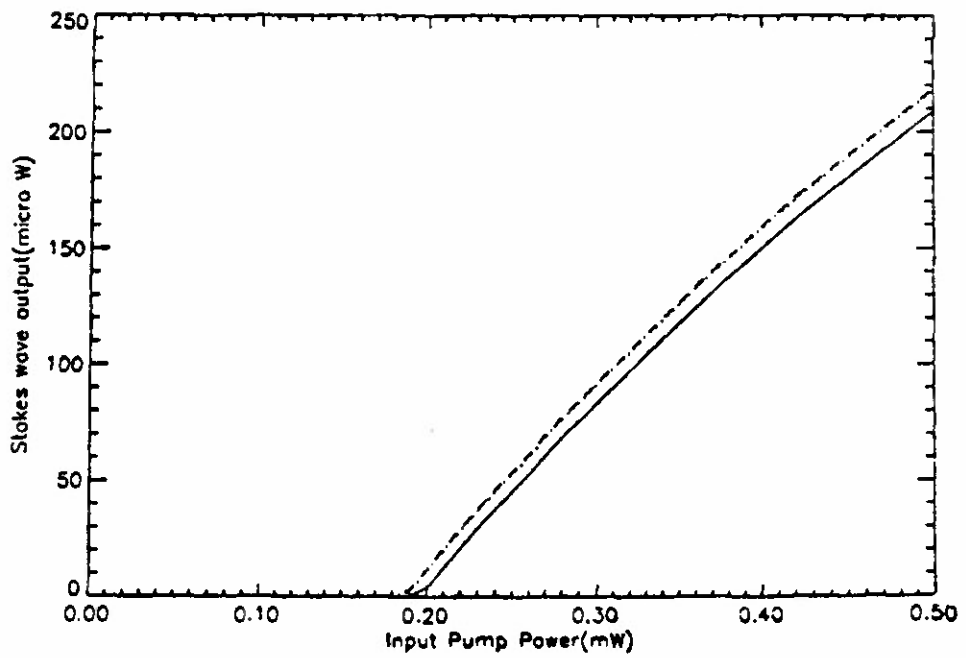
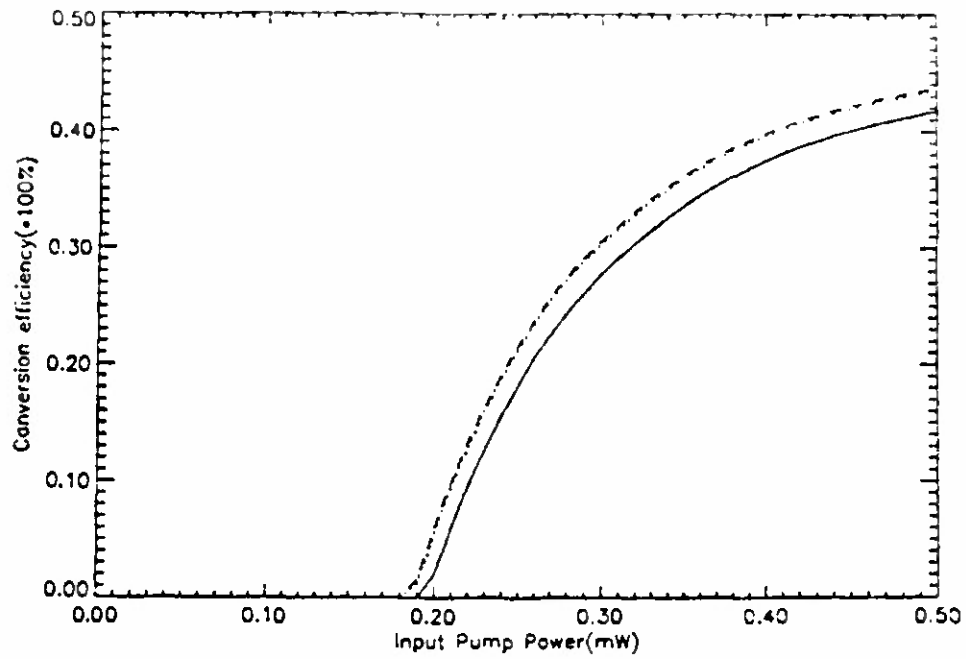


Fig.4.4 (a) Output Stokes power, (b) Conversion efficiency versus the input pump power, with varying fiber loss, at  $1.55\mu\text{m}$ :— $2\alpha_0=10\text{dB}$ , ... $2\alpha_0=1\text{dB}$ , -- $2\alpha_0=0.1\text{dB}$

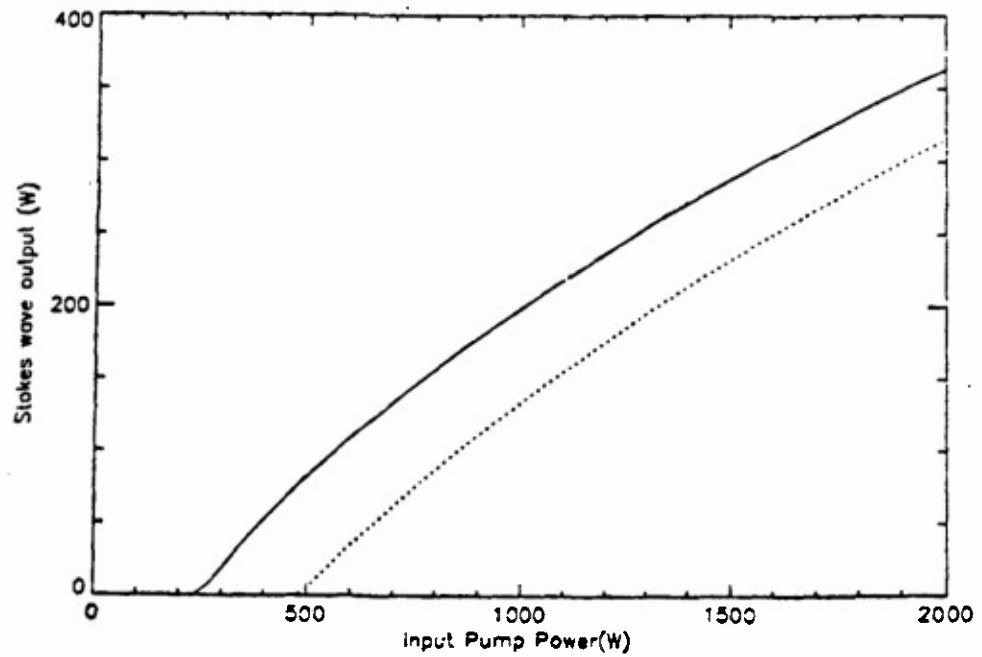
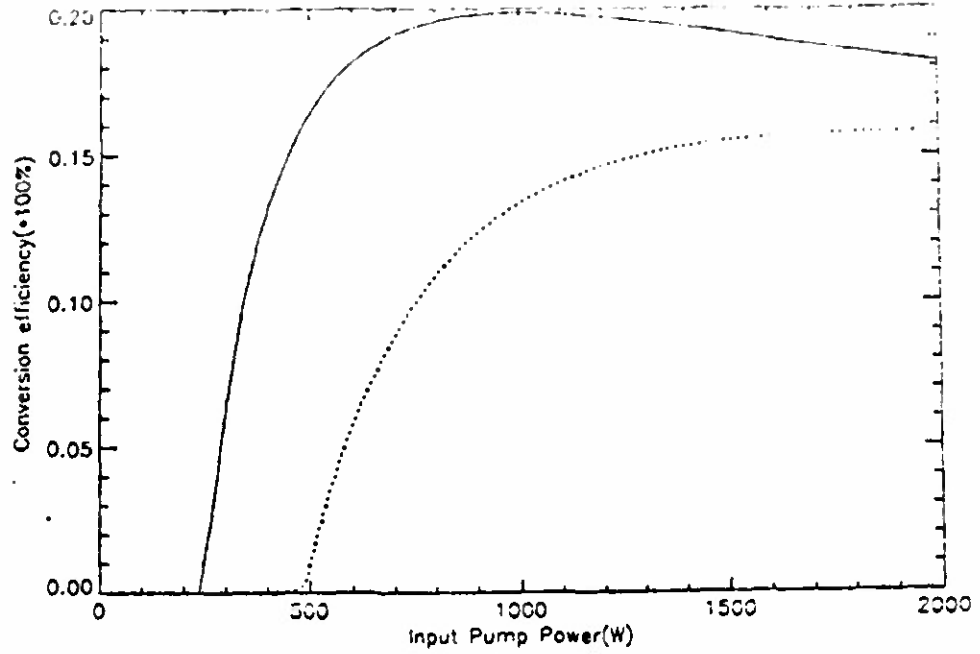


Fig. 4.5 (a) Output Stokes power, (b) conversion efficiency versus the input pump power, with varying coupler loss  $2\gamma$ , at  $10.6\mu\text{m}$ : —  $2\gamma = 0.5\text{dB}$ , ...  $2\gamma = 1\text{dB}$

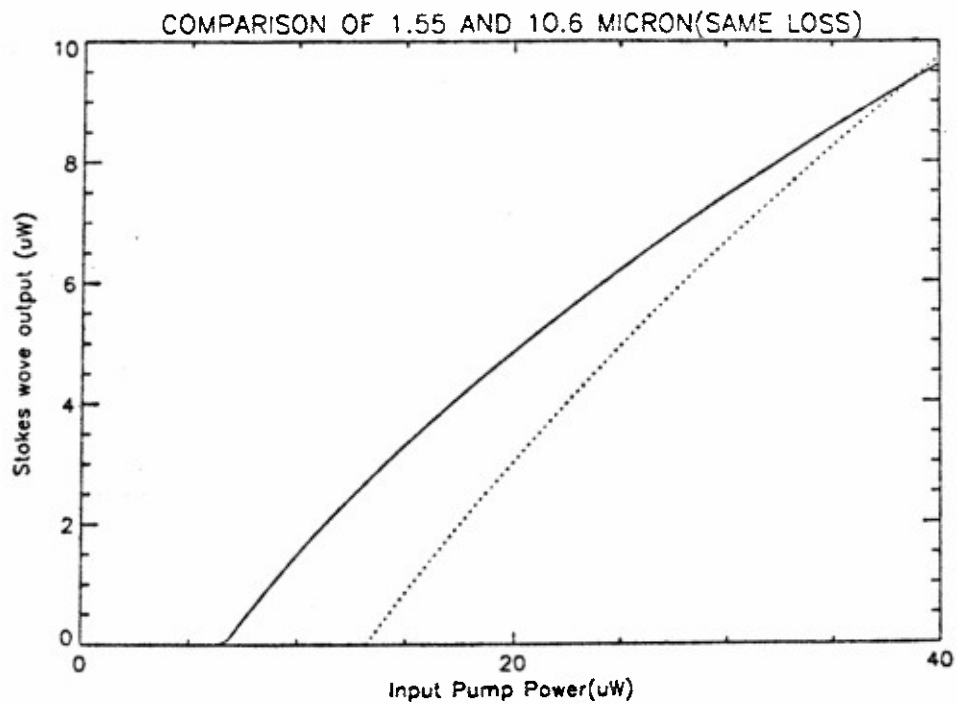
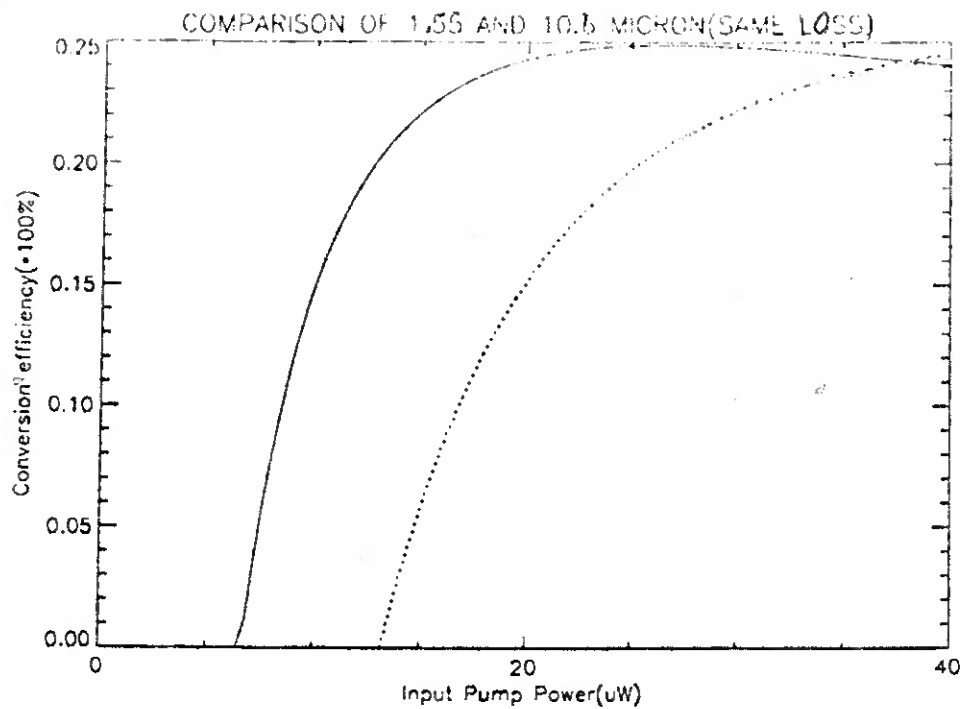


Fig. 4.6  $2\alpha=0.2\text{dB/km}$ ,  $L=1\text{m}$ ,  $2\gamma=0.01\text{dB}$ ,  $K^2=0.9976$ , —  $10.6\mu\text{m}$ , ...  $1.55\mu\text{m}$

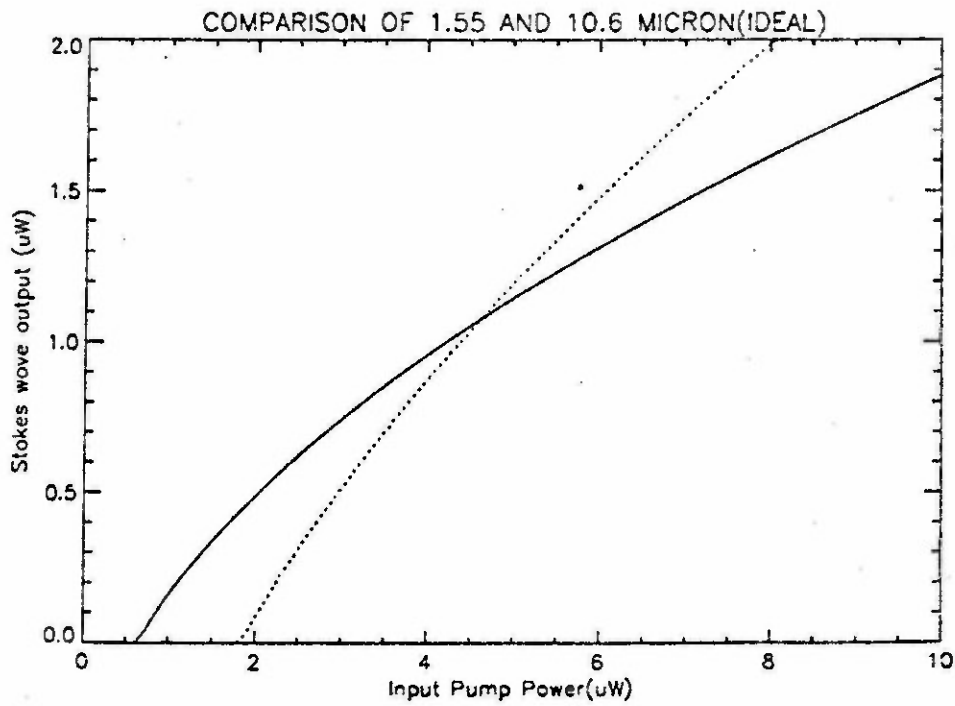
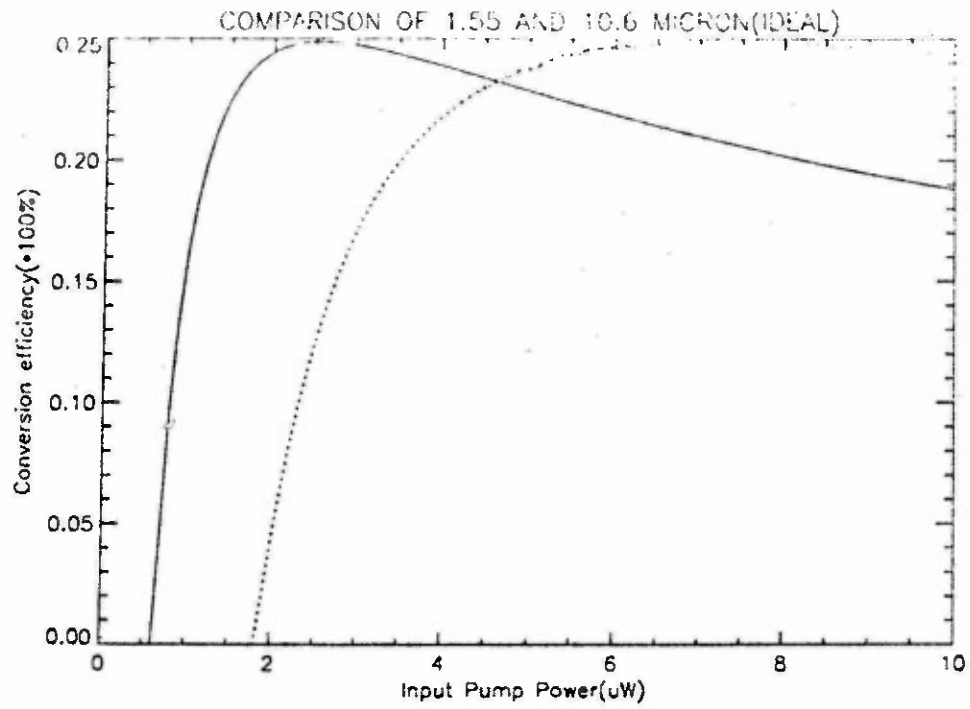


Fig. 4.7  $L=1\text{m}$ ,  $2\gamma=0.01\text{dB}$ ,  $K^2=0.9976$ ,  
 —  $10.6\mu\text{m}$ ,  $2\alpha=0.0002\text{dB/km}$ ; ...  $1.55\mu\text{m}$ ,  $2\alpha=0.2\text{dB/km}$ ;

Table 4.3 Effect of fiber ring parameters to its performance

PARAMETERS OF FIBER RING		PERFORMANCE	
		SBS threshold $P_{th}$	Conversion efficiency $\eta_{max}$
Coupling coefficient $k^2$	$k^2 \leq k_{res}^2$	↑	↑
Loop length $L$	$L < 10m, \uparrow$	-	-
Effective area $A_{eff}$	$A_{eff} \uparrow$	↑	↑
Coupler loss $\gamma$	$\gamma \downarrow$	↓	↓
Fiber loss $L_{oss}$	$L_{oss} \downarrow$	↓	↓

Table 4.4 SBS threshold reduction at 10.6  $\mu m$

Conditions	Linear fiber structure	Ring with current metal halide fiber	Ring with same loss as fused silica fiber at 1.55 $\mu m$	Ideal low loss fiber ring
Fiber radius( $\mu m$ )	500	500	12	12
Loss(dB/km)	1000	1000	0.2	0.0002
SBS threshold	20 kW	200 W	7 $\mu W$	< 1 $\mu W$

## BIBLIOGRAPHY

1. C.K.Fong, "Interaction of externally injected radiation with laser induced SBS phonon in Mid IR fiber", Master Thesis, 1989.
2. — C.Yu, Yat C.Chong, C.K.Fong, "Probe and enhancement of SBS based phonon in infrared fibers using waveguide coupled external radiation", SPIE Vol. 1048 Infrared Fiber Optics, pp. 161-168, 1989.
3. R.G.Smith, "Optical power handling capacity of low loss optical fibers as determined by Stimulated Raman and Brillouin Scattering", Applied Optics, Vol. 11 (11), pp. 2849-2494, 1972.
4. V.I.Kovalev, P.A.Mikheev, and F.S.Faizullof, "Nonlinear scattering at 10.6  $\mu\text{m}$  in a fiber waveguide made of KRS-5", Sov. J. Quantum Electronics, Vol. 14 (8), pp. 1022-1023, 1984.
5. V.I.Kovalev, M.A.Musaev, F.S.Faizullof, and A.K.Shmelev, "Stimulated Brillouin Scattering gains and decay times of hypersonic waves in optical crystal at the 10.6  $\mu\text{m}$  wavelength", Sov. J. Quantum Electronics, Vol. 14 (1), pp. 110-112, 1984.
6. W.Kaiser and M.Maier", Stimulated Raleigh, Brillouin and Raman Spectroscopy", in Laser Handbook Vol. 2, American Elsevier Publishing Co., pp. 1078-1150, 1972.
7. A.Corvo and A.Gavrielides, "Forward Stimulated Brillouin Scattering", J. of Applied Physics, Vol. 63 (11), pp. 5220-5227, 1988.
8. V.S.Starunov and I.L.Fabelinskii, "Stimulated Mandel'shtam-Brillouin Scattering and Stimulated Entropy (temperature) scattering of light", Sov. Physics Uspekhi, Vol. 12 (4), pp. 463-489, 1970.

9. J.A.Harrington, "Crystalline Infrared Fibers", SPIE Vol. 266, pp. 10-15, 1981.
10. S.Sakuragi, M.Saito, Y.Kubo, K.Imagawa, and K.Kotani, "KRS-5 optical fibers capable of transmitting high-power CO<sub>2</sub> laser beam", Optics Letter, Vol. 6 (12), pp. 629-631, 1981.
11. K.Takashi, N.Yoshida, and M.Yokota, "Silver Halide polycrystalline fibers for transmitting high power CO<sub>2</sub> laser beam", 4th Int'l Conf. on Integrated Optics and Optical Fiber Communication, 1983.
12. K.Takashasi, N.Yoshida, M.Yamauchi, "Silver Halide for transmitting a CO<sub>2</sub> laser beam", SPIE Vol. 843, pp. 143-147, 1987.
13. S.E.Hodges, and J.D.Carpenter, "Spectral properties of several infrared transmitting fiber optics", SPIE Vol. 618, 1986.
14. A.Sa'ar, N.Barkey, F.Moser, I.Schnitzer, a.Levite, and A.Katzir, "Optical and Mechanical properties of Silver Halide fibers", SPIE Vol. 843, pp. 98-104, 1987.
15. C.Yu, and C.K.Fong, "Investigation of Stimulated Brillouin Scattering in Mid Infrared fibers", SPIE Vol. 843, pp. 112-117, 1987.
16. Y.Aoki, and K.Tajima, "Stimulated Brillouin Scattering in a long single mode fiber excited with a multimode pump laser", J. Opt. Soc. Am.B, Vol. 5 (2), pp. 358-363, 1988.
17. T.T.Basiev, E.M.Dianov, A.Ya.Karasik, A.V.Luchnikov, S.B.Mirov, and A.M.Prokhorov", Stimulated Mandel'shtam-Brillouin Scattering in a multimode glass fiber lightguide", JETP Lett., Vol. 36 (5), pp. 104-106. 1982.

18. R.M.Shelby, M.D.Levenson, P.W.Bayer, "Guided acoustic wave Brillouin Scattering", *Physical Review B*, Vol. 31 (8), pp. 5244-5252, 1985.
19. L.J.Auchterlonie, A.J.Harris, M.J.Sacco, M.Herbert, J.Lundal, "The detection of microwaves by optical fibers - A new device for measuring microwave power", 17th — European Microwave Conference, 1987.
20. L.J.Auchterlonie, A.J.Harris, and M.J.Sacco, "A novel intrinsic multimode fiber-optic sensor for the detection or monitoring of microwave power", *J. of Lightwave Technology*, Vol. Lt-5 (7), 1987.
21. J.A.Staniforth, Microwave Transmission, Wiley, 1972.
22. J.C.palais, "Fiber Optic Communications", pp. 193, Prentical-Hall, Ina., Englewood Cliffs, 1984.
23. C.L.Tang, (1986), *J. of Appl. Phys.*, 37, 1945-1955.
24. R.H.Stolen, E.P.Ippen, and A.R.Tynes, (1972), *Appl. Phys. Lett.*, 20, pp. 62-64.
25. M.P.Petrov, and E.A.Kuzin, (1983), *Fiz Tverd. Tele.*, 25, pp. 334-338, (in Russian). English transl. in *Sov. Phys. Solid State*.
26. M.P.Petrov, and E.A.Kuzin, (1985). Reprint of A.F.Ioffe Physical Technical Institute, No.975, Leningrad.
27. S.D.Smith, "Optical bistability, photonic logic, and optical computation", *Applied Optics*, Vol. 25, No.10, may 1986.
28. R.W.Keyes, "Thermal limitations in optical logic", *Applied Optics*, 8 (12), Dec 1969, pp. 2549-2552.

29. S.D.Smith, A.C.Walker, B.S.Wherrett, F.A.P.Tooley, etc., "Cascadable digital optical circuit elements in the visible and infrared: Demonstration of some first all-optical circuits", *Applied Optics*, Vol. 25, No.10, May, 1986.
30. J.D.Meindl, "Chips for advanced computing", *Scientific American*, 257 (4), POct 1987, pp. 32-39.
31. K.C.Saraswat, and F.Mohammadi, "Effect od scaling of interconnections on the time deley of VLSI circuits", *IEEE tran. Electron Devices* ED-29 (4), apr 1982, pp. 645-650.

## PUBLICATION RESULTING FROM THE GRANT

1. C.Yu, C.S.Tan, "Minimization of Heating Effects of a Mechanically Stable MOM Point Contact Diode for High Power CO<sub>2</sub> Laser Detection", Submitted to the 13th Intern. Conf. on Infrared and MM Waves, Dec. 5-9, 1988, Honolulu, Hawaii.
2. C.Yu, Yat C.Chung and C.K.Fong, "Probe and Enhancement of SBS Based Phonons in Infrared Fibers Using Waveguide Coupled External Radiation", Pres. at SPIE's OE/Laser '89, Medical Applications of Laser and Optics, Jan. 15-20, 1989, Los Angeles, CA.
3. C.Yu, Yat C.Chung, Hongyi Zhou, "Study of Mid Infrared Fiber Transmission and Mode Patterns Under Laser Induced Stimulated Brillouin Scattering", Presented at LASER '89 Conf., New Orleans, LA, Dec. 3-8, 1989.
4. Chung Yu, Yat C.Chong, Hongyi Zhou, and Haishan Zhou, "Theoretical Considerations of SBS Based All-Optic Switching and Amplification for Computing and Communications Applications", The 1st Annual Symp. on CSA, March 22-23, 1990, Greensboro, NC.
5. C.Yu, and Haishan Zhou, "In Line SBS Based Multi-Channel Near IR Fiber Optic Device for Amplification, Switching and Channel Selection", 15th Intern. Conf. on Infrared and MM Waves, Orlando, FL, Dec. 10-14, 1990.
6. Haishan Zhou, and Chung Yu, "Preliminary Studies of the Fiber Ring for Enhancement of SBS Generation in Mid Infrared Fibers", The 2nd Annual Symp. on CSA, March 21-22, 1991, Greensboro, NC.
7. Annette Holliday, and Chung Yu, "Suppression of Noise in Fiber Amplifier by Fiber Ring", The 2nd Annual Symp. on CSA, March 21-22, 1991, Greensboro, NC.

8. C.Yu, Annette Holliday, and Haishan Zhou, "The Fiber Brillouin Ring for Low Noise Amplification, Switching and Channel Selection", 23rd Southeastern Symp. on System Theory, Columbia, SC, March 10-12, 1991.
9. C.Yu, Haishan Zhou, and Swee Cheng, "Optical Fiber Brillouin Noise Amplification for Sensing", Presented at Lasers'91, San Diego, CA, Dec. 8-13, 1991.
10. Swee Cheng, Haishan Zhou, and Chung Yu, "Fiber Brillouin Ring Laser for Active Internal Rotation Sensing", Presented at 24th SSST, Greensboro, NC, March 2-3, 1992.
11. Haishan Zhou, Swee Cheng, and Chung Yu, "Experimental Investigation of the Optical Noise Sensing Capabilities of the Brillouin Fiber Ring Amplifier", Presented at 24th SSST, Greensboro, NC, March 2-3, 1992.
12. Chung Yu, Haishan Zhou, and Swee Cheng, "Near and Mid IR Fiber Brillouin - Active Optical Devices and Applications", 25th SSST, Tuscaloosa, AL, March 1993.

SCIENTIFIC PERSONNEL SUPPORTED DIRECTLY OR INDIRECTLY BY THE  
GRANT

1. A. Niczad --- MSEE degree (1986);
2. M. A. Hemmatian --- MSEE program in progress;
3. A. Yekrangian --- MSEE degree (1986);
4. C. K. Fong --- MSEE degree expected 1987;
5. C. S. Tan --- MSEE degree expected 1987;
6. A. Sabzali --- MSEE degree (1987);
7. F. Flores --- MSEE degree expected 1988.